Hollow fiber based pre-concentration and a microfluidic filtration device for water samples

Hollow fiber based pre-concentration and a microfluidic filtration device for water samples

By

Lee J. Peter, B.A.Sc.

A Thesis

Submitted to the School of Graduate Studies

in Partial Fulfillment of the Requirements

for the Degree

Master of Applied Science

McMaster University

Hamilton, Ontario, Canada

MASTER OF APPLIED SCIENCE (2013) McMaster University

(Biomedical Engineering) Hamilton, Ontario, Canada

TITLE **Hollow fiber based pre-concentration and a microfluidic filtration device for water samples**

AUTHOR Lee J. Peter, B.Sc.

SUPERVISOR Dr. P. Ravi Selvaganapathy, Professor

Department of Biomedical Engineering

NUMBER OF PAGES xiii, 99

ABSTRACT

Sample preparation is a crucial processing step required for molecular biological analysis of environmental samples like water that has a variety of constituents in it. Furthermore, large volumes of sample need to be processed as the prescribed limits of pathogens in water are extremely low. However, microfluidic biosensing devices that can perform rapid molecular biological analysis in the field are designed to handle small sample volumes. In such cases, there is a need for a sample processing device that can reduce (concentrate) a large sample volume into a small one while retaining the biological species present in it. Hollow fibers are appropriate for this purpose of sample reduction and serve as a macro to micro interface for the microfluidic device. The received concentrate from the hollow fiber device requires be further concentrated to several microliters and separated and sorted to various modular components within the microfluidic device. This requires a second stage microfiltration where an integrated membrane can sort based on particulate size. In this thesis, a two stage filtration was designed.

A first stage hollow based fiber pre-concentration device is developed that is portable, low cost, has high retention efficiency, low elution volume and is rapid. The hollow fiber device has low elution volume of ~1-3 ml. Controlled experiments were performed to validate the recovery of the hollow fiber device. Simulated 250 ml *E.coli* contaminated samples were filtered to <5 ml from an original sample volume of 250 ml. No bacteria were present in the filtrate and nearly 100% was recovered at high bacterial concentrations. At low concentrations (~200 cells in the sample) the recovery was less (~50%).

A second stage microfiltration device that can be integrated with the microfluidic device and that can reduce the sample still further from ~ 5 ml to 5 µl was designed. Plasma bonding of

ultrafiltration and microfiltration membranes using fluorine ions was investigated for fabrication of this device. The bonding of PDMS channels with polysulfone membranes via SF_6 plasma was tested via tensile pull tests, burst pressure tests, and analyzed through scanning electron microscopy and electron dispersive x-ray spectroscopy. Quantitative tests on 10kDa and 70kDa polyethersulfone membranes demonstrated increased operational bonding strength of 86.6 and 146.9 kPa increases with three hour plasma application. Microfiltration membranes (0.2 micrometer pore size polyethersulfone) bonded in such a way that was easier to permeate as compared to ultrafiltration membranes. This bonding technique is generic in nature and can be used for integration of other commercially available polyethersulfone membranes with microfluidic devices for applications such as bio separations. No filtration testing was performed with *E.coli* samples.

ACKNOWLEDGEMENTS

Academic research has been an enlightening experience in which I have learned many valuable life lessons. My greatest and humblest gratitude is given to Dr. Ravi Selvaganapathy. His guidance and encouragement as well as insight and vision provided to me during this project have given me the strength to finish this academic marathon. His mentorship has cultivated excellent research within the entire lab including myself.

Special thanks for being patient with me while giving reviewing my original draft of my thesis. I greatly appreciate this academic experience he has provided me which will provide opportunities and prepare me for challenges within the future. I cannot thank him enough.

In similar context, I gratefully thank Dr. Chan Ching for substituting as supervisor in Dr. Ravi Selvaganapathy sabbatical. He provided exceptional and unique guidance in his absence.
I thank the many collaborators who have warmly opened their labs and resources to us.

Special thanks to Dr. Bhagwati Gupta and the entire *C. elegans* lab for training me and providing me with lab space to operate. Special thanks to Siavash Amon and Justin Tong for assistance.

Special thanks to Dr. Jamal Deen and Fangfang Zhang for their collaboration with me on investigating plasma bonding techniques and help operating the Instron testing.

Special thanks to Dr. Raja Ghosh and Seungmi Yoo for providing PES Membranes and Polyproprelene hollow fibers as well as special guidance in theory behind membrane.

Recognition goes my labmates, Shehad, Leo, Ali, Bo, Pouya, Micheal, Siawash, Reza, Russel, Wen, Jackie, Bala, and Salman for providing an exceptional and interesting work environment. To my family, thank you for your support of me throughout this process.

TABLE OF CONTENTS

LIST OF TABLES

LIST OF FIGURES

Chapter 1 Motivation and Organization

1.1 Motivation

Water is an essential need for survival but around 35% of the deaths worldwide are a direct result of water-borne diseases or contamination (World Health Organization Report 2009). Diarrheal diseases are second leading in mortality in low-income countries and fifth in general. An important but overlooked aspect of combatting water-borne diseases is detection of contamination in water sources. Conventional methods for detection such as colony morphology identification of water borne diseases are not timely due to multiple samplings at different sites, sample transport to a testing facility and incubation time for amplification. This time delay endangers people who require safe drinking water especially in areas where well water is the main source of drinking water. Currently, health hazard warnings for swimming in lakes in Canada are posted two to three days after sampling. Moreover, conventional methods may not detect all viable pathogens because some may be in a non-cultivable state. Therefore, a need for on-site accurate detection method without incubation time is required. Molecular biology approaches may meet most of these demands considering they are fairly accurate, extremely sensitive and timely (in a few hours). Potentially, it can be a viable method for detection. Several detection methods using molecular biology exploit the deoxyribonucleic acid (DNA) hybridization process to identify certain sequences linked to pathogenic species [1], [2], [3]. However, molecular biology techniques require laboratory processes and equipment for their purification, amplification, and detection which are expensive, immobile and may not be accessible especially in low-income countries. In the recent two decades, a large effort of

miniaturization of lab processes onto a single chip has been investigated. Small biosensors coupled with the molecular biological identification are becoming desirable since biosensors can perform the same function of detection with a single, portable, and inexpensive chip [4], [5], [6]. Several biosensors have been developed using various detection modalities but there are typically two main types: optical and electrochemical [7]

Optical detector types are commonly developed using fluorescent microarrays [8]. Microarrays require fluorescent tags to attach to unhybridized DNA in microwells or microdots. The unhybridized single stranded DNA containing sequences of a variety of pathogenic bacteria is attached to each individual well or dot. Therefore, a single dot or well will sense one pathogen. In an experiment, the pathogenic bacteria that requires detection has its DNA or ribonucleic acid (RNA) extracted and amplified through polymerase chain reaction (PCR).

After PCR, the pathogenic single strained DNA or RNA is attached to fluorophores to the end of the strains making fluorescent tags. The target pathogenic RNA/DNA tagged with fluorophores is washed over the microwells/dots allowing the target pathogenic DNA to hybridize with the corresponding sequence in a well/dot. The excess pathogenic DNA is rinsed away and the microarray is exposed to UV light causing excitation of the fluorophores attached to the pathogen DNA. The well or dot fluorescing determines the presence of the pathogenic bacteria within the sample. Microarrays are single use devices since the microarray wells/dots cannot be replaced once used. Electrochemical methods typically use field-effect transistors coupled with pathogenic DNA tags attached to a gate electrode to detect pathogenic bacteria. The attachment of DNA through hybridization creates a change in electrical signaling which can be detected. The signal usually can be amplified by nanoparticles as an intermediate between sensor and DNA [4], [9].

Both the optical and electrochemical sensors require samples in a purified form of DNA with minimal interferences with other chemical species. However, in reality samples are never "clean" and often have a variety of biological, chemical contamination and material particulates. The biological or chemical contamination and particulates could interfere with DNA hybridization either by blocking the site of attachment or interfering with the electrical sensing. Consequently, a variety of processing steps are required to extract and deliver the target bacterial DNA to the biosensor as an acceptable sample. The steps required are typically filtration / concentration, cell processing, DNA extraction and amplification. Filtration / concentration typically remove the large and smaller particulates to isolate the specific bacteria. Cell processing is required to lyse the bacterial cell membrane and release the cellular material. DNA extraction is needed to separate the DNA from proteins, lipids and the rest of the cell lysate. In addition, amplification of isolated DNA can be performed if the concentration is low or undetectable. The first step of filtration / concentration is the most crucial step in sample processing as pathogenic bacteria or viruses are present in low concentration in water.

According the US EPA, the maximum amount of coliforms in drinking water is 5.0 mg/L. This level is only to indicate an acceptable level of bacteria since not all bacteria is pathogenic. In drinking water, the maximum limit for *E.coli* is zero in 100 ml and the maximum infectious dose of *E.coli* is ~10 cells in 100 ml [10].

Therefore, one requires ways to increase the amount of detectable bacteria from a small infectious dose. The most common and conventional way to increasing the detectable level of bacteria is enrichment. Drinking water samples are seeded into Lysogeny broth (LB) growth medium or seeded directly onto a LB-agar plate and incubated to multiply any bacteria present indiscriminately.

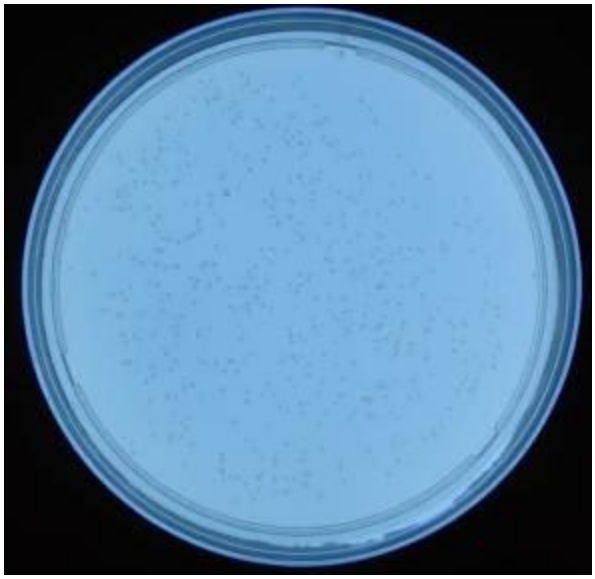

Figure 1: Plated *E.coli* on LB-Agar petridish commonly used in detection of bacteria

If not already plated, the bacteria is seeded onto a LB-agar petridish and identified by colony formation since bacterial types can be identified by colony morphologies in petridishes seen in Figure 1. Enrichment is a well-defined method for binary determination of detection but poorly describes the level of contamination. Furthermore, enrichment requires approximately 16-24h for incubation.

An alternative to enrichment would be concentration. Concentration simply takes a large sample size and reduces the volume of water, thus concentrating the sample. Assume that a large body of water such as a well or lake is contaminated and a sample is taken which represents the sample source seen on the left of Figure 2. Any small sample from this source will have only a minute amount of bacteria since the concentration of the lake is same as the sample. If the sample size is too small, then the bacteria in the source may not be detected even in a sophisticated biosensing device. Therefore, it is necessary to take a large sample and concentrate it down to the ml-μl range rapidly so it can be analyzed by a microfluidic DNA sensor (lab-on-a-chip device). Lastly, another filtration setup within the microfluidic device in various stages will

separate/categorize the filtrate into bacteria, other analytes such as heavy metals and waste. Thus, a two-stage filtration setup is required for a microfluidic sample; one macro for concentration and reduction and one micro for filtration and separation.

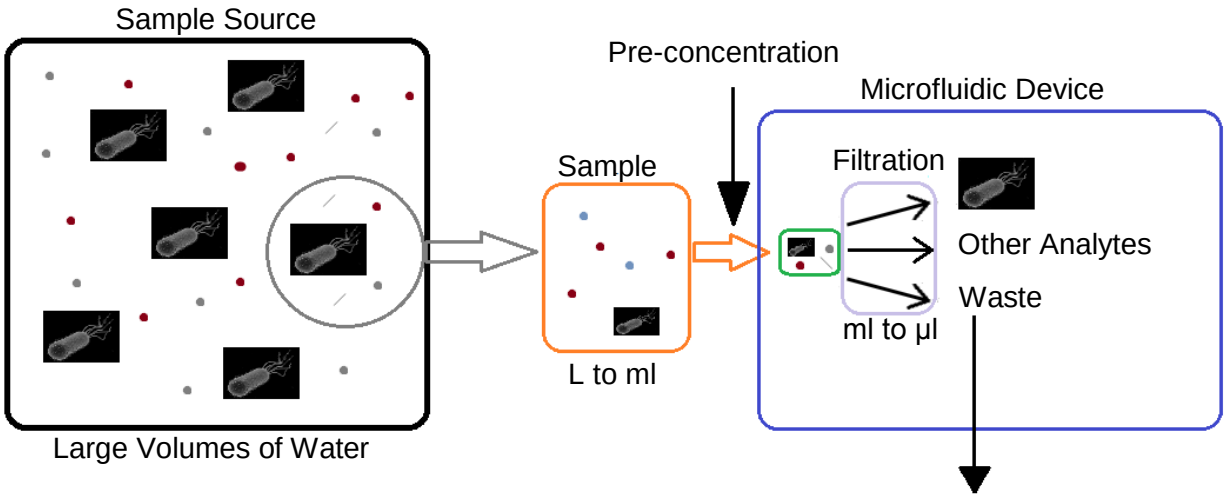

Figure 2: Schematic diagram explaining pre-concentration for a lab-on-a-chip device

The thesis will focus on two stages of filtration based on this basic design. One large macro-scale concentration process ex-vivo of the micro fluidic device and one in-vitro integrated filtration process part of the microfluidic device.

1.2 Organization of Thesis

The structure of the thesis is separated into components and organized in chapters.

Chapter 2 provides an overview of analysis of detection methods for bacteria DNA and review of conventional analytical detection methods. An expanded discussion of detection methods via lab-on-a-chip and a concise discussion on sample refinement are presented.

Chapter 3 presents the design, fabrication, and performance of an ex-vivo macro-scale pre-concentration device.

Chapter 4 is the design and fabrication of a filtration step into a microfluidic device and focus on integration method, refinement, and improvement of integration.

Chapter 5 concludes the thesis by emphasizing the contributions of this research. A number of suggestions for future development of the device and research directions are proposed.

Chapter 2 Introduction

2.1 Overview of Conventional Detection

Identification of type of bacteria has many different applications in research, food/water and medical diagnostics. Traditional bacterial identification is performed by observation of colony morphology to determine phenotype [11]. Samples are usually collected from various sources and cultured in a nutrient saturated source filled with nitrogen, oxygen, carbon, salts and vitamins in an enrichment process. After enrichment for a day, some of the sample is streaked onto a plate using a swab. Plates are incubated within an incubation chamber to cause bacteria to multiply at an exponential rate. After plating, basic phenotype identification is performed accounting for environmental requirement for growth, resistance or susceptibility to antimicrobial agents, nutritional requirements and metabolic capabilities, and microscopic morphology and staining characteristics. Colony morphology is determined by a macroscopic inspection of colonies based on size, shape, color, topology and surface appearance seen in Figure 1. This morphological determination can be compared to a database that consists of morphological features of known bacterial species and sub-types. Microscopic morphology via visual identification under microscope is inspected in addition to colony morphology. Under microscopic morphology, bacteria are identified by size, shape, arrangement alongside gram staining and acid fast testing.

Although colony morphology is simple to identify presence of specific bacteria such mTEC agar plates for *E.coli*, it is cumbersome and time consuming to identify multiple types of bacteria in one sample. Furthermore, the incubation times for plating increase the detection time

to two to three days. Lastly, anaerobic bacteria or viruses would not be detectable via this method since these are non-culturable pathogens.

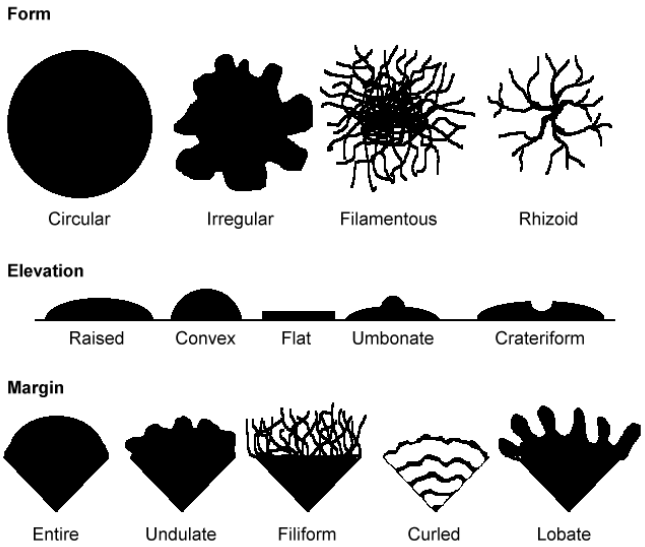

Figure 3: Colony morphologies (www.sciencebuddies.org)

Molecular biology-based approaches started to develop in the middle of the last century and genomic sequences for various types of bacteria strains were mapped. The invention of DNA amplification using polymerase chain reaction (PCR) created a new detection method of bacterial strains using genotype.

The genotype detection method requires bacteria strains after plating using conventional methods aforementioned. Bacteria are lysed using chemical surfactant such as Triton X or SDS, DNA is extracted and purified via centrifugation. DNA extracted is uncoiled via proteinase K enzyme and broken into specific pieces through DNA digestion enzymes.

DNA fragments are amplified using PCR using a thermal cycler in which it rotates through hot and cold cycles doubling the DNA every time. After amplification, DNA fragments are stained with fluorescent dye such as ethidium bromide and are separated based on their size by gel electrophoresis. The DNA fragments can be compared to a pre-set ladder of DNA

fragment lengths. A DNA fragment usually unique to a species of bacteria (gene encoding 16S ribosomal RNA) is selected to be amplified and compared to a database (NCBI's database) to identify the specific bacteria.

Considerable amount of equipment and unit operations are required for genotyping which can be costly requiring trained technicians and expensive equipment such as autoclaves (sanitation), centrifuges (separation), incubators (growth), thermal cyclers (PCR), DNA sequencers, and gel electrophoresis (gel encasing, power supply).

Even though molecular methods are faster in analysis they still require enrichment phase to grow very low concentrations of pathogenic bacteria that may be present in the sample. This enrichment phase leads to long waiting times of typically 48 to 72 hours [12].

Table 1: Estimated times for genotyping method

Equipment	**Time (H)**
Autoclaving	1-3 per sanitation
Centrifuging	Few minutes
Incubation	16 – 24
PCR	Depends on thermal cycling
Gel Electrophoresis	1-2
DNA Sequencing	Depends on type of sequencing and base pair length. (Sanger method 20 minutes to 3 hours)

2.2 Introduction to Microfluidics

Microfluidic devices are designed to accept microliter-sized sample volumes and process or analyze the samples to provide an output usually in the form of information on the biological or chemical content of the sample. Microfluidics is a promising field in genotyping technology where a number of problems associated with conventional detection techniques can be mitigated. Advantages such as reduced sample required and reduced extraneous reagents are some of the

benefits from microfluidic system. Microliters of samples are required for sensing which is advantageous when large sample collection is a major issue.

The applications to cell biological samples in microfluidics are a natural fit together since most cells are 1 μm -100 μm size range, fluidic based and usually are available in small sample volumes that are conducive for microfluidic system [13]. Currently, there are microfluidic devices designed and developed to sort cells, lyse cells, separate DNA through electrophoresis, mix and separate fluids, amplify DNA through microPCR, perform enzyme assays, perform immunoassays, and count DNA, bacterial, blood and tissue cells through cytometry [3], [4], [5], [6].

A combination of sensors based on genotype technique with several processing steps listed above can create a single all-in-one device that can potentially detect bacteria present in a sample. An example of a detector is BioFETs. BioFETs are fabricated by attaching single stranded (ss) DNA probes of bacteria (such as *E.coli)* specific DNA sequences to the functionalized gate oxide of the field-effect transistor (FET) seen in Figure 4. When *E.coli* specific DNA sequences in the sample hybridizes, the negative charged backbone of DNA doubles the charge on the gate between the source and drain which changes threshold voltage of the FET resulting in detection mechanism for DNA [9].

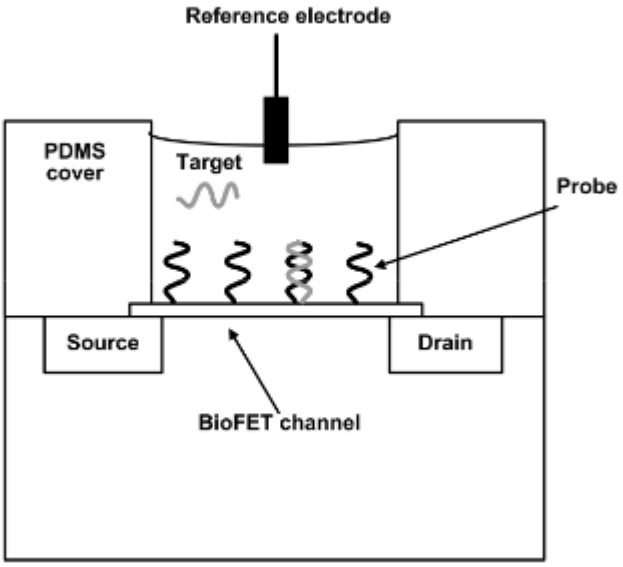

Figure 4: Simplifed BioFET diagram [9]

A majority of the existing biological sensors cannot handle raw samples and require manual sample preparations or cleaned samples with concentrated amounts of target material [17] ,[18].

For example in blood samples, a cell lysis and separation device using capillary electrophoresis required centrifugation of the sample at 1000 rpm for 5 min to separate the sample erythrocytes and resuspended to make a high concentration solution (1.2×10^5 cells/ml) [19]. Another device for cell lysis, protein extraction and fluorogenic enzyme assay targeting bacteria used a prepared suspension of *E.coli* cells (~10^8 cells/mL) and 1 mL/mL Bacterial Protein Extraction Reagent for protein extraction [20]. In microPCR chips, samples must be prepared by manually mixing magnesium salts, pH buffer, and potassium salts, DNA substrates, oligonucleotide primers, polymerase enzyme, and dNTPs and introduced into the chip to perform amplification [21].

More recently, investigations on integration of multiple sample processing have been attempted. For instance, a self-contained biochip for sample preparation, PCR amplification, and DNA Microarray Detection of *E.coli* (10^3–10^6 *E.coli* K12 cells) in rabbit blood has been developed [22]. The sample processing step consists of a magnetic bead based capturing mechanism that captures the *E.coli* cells in the sample blood as it is flowed through a capture chamber. Although promising, the concentration of *E.coli* used is high and unlike real life sample, and manual sample preparation was done prior to injection into the device. Also, the reagent addition at each step was manual [18].

Moreover, many of the microfluidic sample preparation devices are designed and developed for handling smaller volumes that are typical in clinical diagnostics from blood and saliva where upon infection the pathogenic concentrations are high and may not be suitable to handle large volume, low concentration samples. Microfluidic biosensors are not designed to handle large-volume low-concentrated real life samples such as water samples and require sample reduction to low volume and high concentration.

Summarizing, a large majority of biosensors require some sort of pre-processing of sample to purify the sample and to increase the concentration to detectable limits. The sample processing is dependent on the type of sample, volume, concentration of pathogens in it as well as the complexity of the matrix.

2.3 Sample Processing for Water Detection

As per the motivation, a portable and fast bacterial detection method is required for drinkable water especially in developing countries. A microfluidic device with a DNA based sensor would be portable and cheap enough in order to satisfy these conditions, but sample

preparation of water is required before loading into a microfluidic system. The sample preparation for bacterial detection in a microfluidic device requires enrichment through incubation to increase the detectable levels of bacteria. Unfortunately, incubation is the longest step required in conventional methods (16-24H) and would eliminate immediate on-site detection. Thus, an alternate method to enrichment is required to increase the amount of detectable bacteria in sample.

The other way of increasing the amount of detectable bacteria is collecting a large sample volume and reducing the volume of liquid eventually concentrating the bacteria compared to incubating seen in Figure 5. Thus, the advantages of concentrating over enrichment are avoidance of 16-24H incubation step and determination of the original concentration accurately assuming that there is no bacterial growth during the sample processing. However, a large volume of sample needs to be processed to obtain sufficient amount of bacteria for detection. Levin *et. al.* [23] successfully concentrated 10- 70 L of tap water using a Baston-type AA filter under vacuum with a 40% to 100% recovery rate usually taking 60 min for 10 L. Goyal *et. al.* [24] used zeta potential filter tube membrane to reduce 20 L to 50 ml with 50-99% recovery rate within 10-40 mins. For larger volumes, S R Farrah *et. al.* [25] filtered up to 1900 L with an average 50% recovery rate using pleated membrane filters for approximately 3 hours.

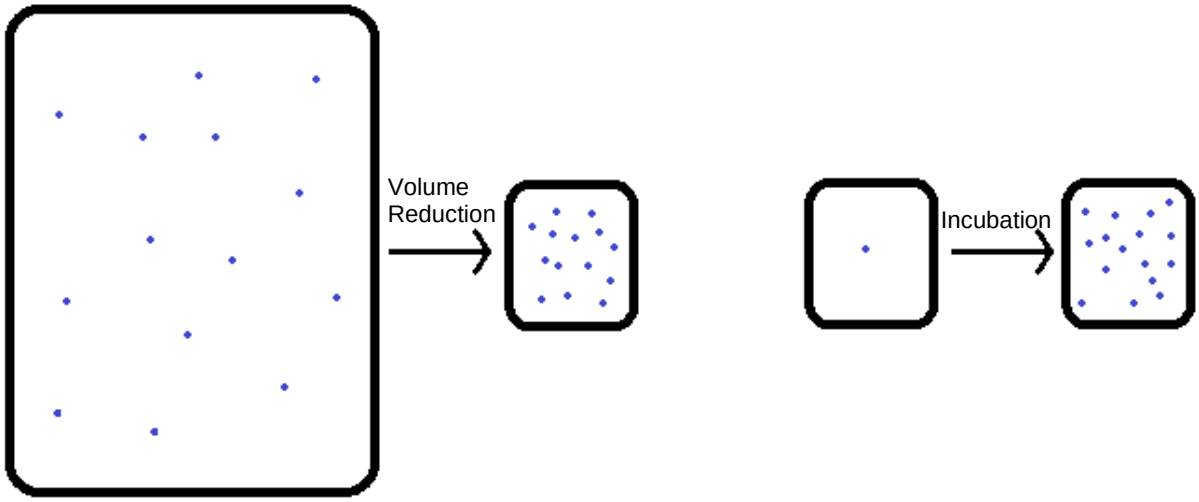

Figure 5: Concentration vs. Enrichment

There are reasons that prevent the use of existing methods in our case. Firstly, although these methods have fast filtration rate with large volumes, none of these systems were designed to be portable as all of them require a peristaltic or vacuum pump therefore requiring a power source to provide enough pressure for the high flow rates. In addition, the infrastructure needed such as pumps, tubing, large glassware, and filters is expensive and occupies a lot of space. Secondly, the filtration methods have varying and inconsistent recovery rates depending on filter type and flow rates. Bacteria retention and release (recovery) is extremely important since pathogenicity occurs at very low concentration. Third, these methods and other similar ones in literature were not designed for microfluidic samples. A large amount of tubing and subsequent eluting reagents caused >5 ml amounts of remaining liquid or dead volume. Dead volume is defined as the volume of the filtration device. An example would be tube fittings and remaining liquid in reservoirs. Dead volume is an important factor since it will directly relate to the amount of volume that will be loaded into DNA sensor.

There are some aspects of these large filtration systems that would be beneficial to keep in a proposed microfluidic designed concentration device. Firstly, the time required to filter the samples were performed under an hour compared to 16-24H for incubation. Any additional time due to the concentration step should be considered since it would add-on more time to the detection step of the DNA sensor. In summary, four main factors will be the main deciding factors in the type of filtration mechanism.

1- Portability & Cost (No pumps, low-cost materials)

2 -Recovery (As high as possible - 100%)

3- Dead Volume (Small as possible - <5 ml)

4- Time (Small as possible - < 1hour)

Based on these considerations the design of a two stage filtration system to reduce sample volumes to be handled by microfluidic devices will be detailed in the next chapter.

As for the amount of liquid to be filtered required, there are two factors contributing to determine: the level of contamination in the water sample and sensitivity of the device receiving the concentrated sample. Depending on how much contamination is in the water sample, the amount of volume to concentrate to detect a pathogen varies. For example, waste water would require almost no concentration compared to drinking water. Assuming that drinking water is the case, ~10 bacteria for 100 ml is the minimum infection dose which will be considered as the lowest detectable concentration required. The device sensitivity of a microfluidic chip depends on PCR as it amplifies the pathogenic DNA. Yang, J *et. al.* [26] and Min J *et. al.* [27] have both shown in high sensitivity micro PCR lab-on-a-chip requiring only 10-100 bacteria in blood. Assuming 10 bacteria in 100 ml, a pre-concentration of volume in-between 100 ml to 1L is required.

Chapter 3 Design of a Hollow Fiber Filtration Device for Pre-Concentration of Bacteria

This chapter outlines the design and characterization of a macro-scale pre-concentration device for preprocessing of water sample to make it suitable for a lab on a chip device (i.e. reduce the sample to <5ml with near 100% recovery). First, the design section describes several criteria pertaining to conventional filtration modules used in macro and ultrafiltration and lists several options for a portable on-site macro-scale pre-concentration device. From the options listed, a suitable method is chosen based on the requirements of the application. The next section determines the device fabrication and experimental process to quantify performance based on selected methods. Subsequently, the results and discussion of the device are presented.

3.1 Device Design

The macro-scale filtration device is designed to reduce the volume of a water sample from 250 ml to 1-2 ml that is suitable for loading on to a microfluidic device without any loss of bacteria in the sample. In choosing a suitable membrane for filtration the following factors such as 1) configuration or shape of the membrane 2) membrane composition and 3) specific pore size should be considered. In addition, the encasing or containment of the pre-concentration device which is determined by the type of membrane used should also be determined. In operation, the flow configuration and the pressure source are factors to be considered.

3.1.1 Membrane Form

A crucial aspect in design of a macro-scale filtration device is the membrane form. There are three forms of membrane: flat sheet, tubular, and hollow fiber. Flat sheet membranes are widely used and are housed in the module made of a top and bottom part that are machined out of hard polymers such as Teflon or HDPE and then clamped together using screws and vices seen in Figure 6. An O-ring is placed in between the membrane and housing to create a seal.

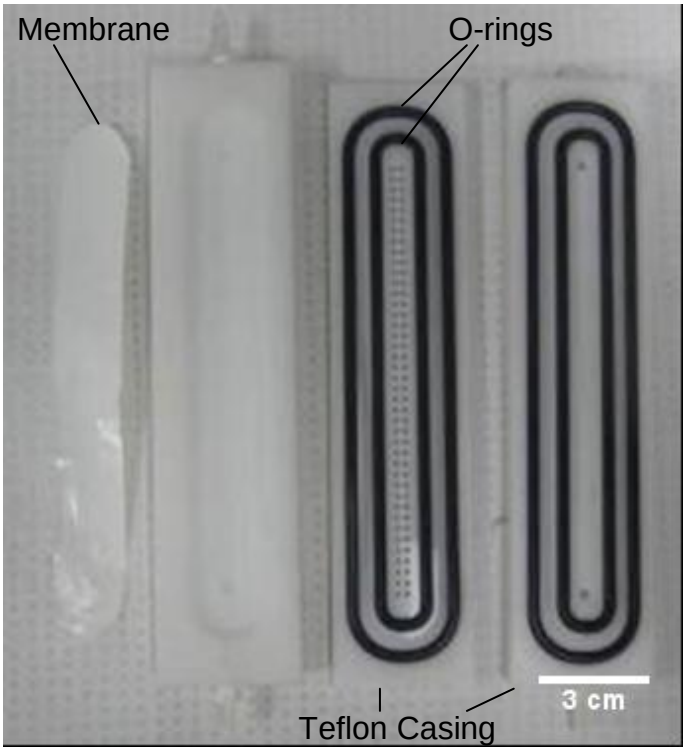

Figure 6: Tangential flow module using flat sheet PES membrane and teflon casing

Although such modules have been used for pre-concentration, the membrane surface-to-dead-volume ratio of such configurations is large. In addition, they require additional pumps to circulate fluid and may not be suitable for a portable device [10]. Although this configuration is useful in various applications in research and in-line production, it is not suitable for a portable and low-cost pre-concentration module.

Tubular membranes are beneficial since they use turbulent flow to increase permeation but still require large encasing due to the large nature of the membrane [28]. Most importantly, the dead-volume to membrane surface area ratio for these configurations is quite low resulting in high amounts of dead volume [28].

Another alternative is the use of hollow fiber membranes. Hollow fiber membranes are small circular tubes, hence the name fibers, where the membrane is either the inner or outer surface of the tube seen in Figure 7. The inner surface of the hollow fiber is referred to the lumen-side and the outer surface is the shell-side. The amount of membrane area to volume is high in comparison to other configurations. For example, comparing flat sheet to hollow fiber, flat sheet surface area to volume ratio is dependent on the module encasing and the amount of surface area. The corresponding surface area can be obtained at a much smaller volume in a hollow fiber. The sample is pushed through axially either inside or outside by negative or positive pressure. The casing can be as simple as a long outer tube with epoxy as a sealant. Also, these hollow fibers have been already used in industrial water purification systems which indicate their suitability for this application. Hollow fibers are typically arranged in bundle form but only one hollow fiber will be tested first to determine its performance.

Figure 7: Commercial microporous polyethylene hollow fibers (www.mrc.co.jp)

3.1.2 Material Composition

Filtration membranes are typically polymeric and can be made of the following materials: polyethersulfone (PES), cellulose acetate (CA), polyvinylidenefluoride (PVDF), polyacrylonitrile (PAN), polycarbonate (PC), polypropylene (PP), polyethylene (PE) and nylon.

Among them, polyethersulfone has various characteristics such as chemical robustness, low and reversible fouling, and high throughput which are desirable [29] in this application. Polypropylene is also very useful since it has high void volumes, well-controlled porosity, chemical inertness, good mechanical strength and low cost [30]. There are small differences between all these materials but the focus would be on these two types mostly since they were the most readily available and widely used. Also, electrically neutral membranes were chosen so that the membranes will not retain bacteria [31].

3.1.3 Pore Size

E.coli bacteria are typically around 2 μm length and 0.5 μm in width with some deformability. It has been demonstrated that membranes with pore sizes between 0.1-0.45 μm are able to retain bacteria through size exclusion [32]. Therefore, a pore size of 0.2 μm was chosen although the pore size is fairly conservative related to bacteria filtration. Larger 0.45 μm pores were not considered since membrane manufactures report 0.45 μm pore size, but realistically membranes have a Gaussian distribution of pore size centered at 0.45 μm which would have some pores allowing *E.coli* to pass through. Pore sizes of 0.1 μm is even more conservative but smaller pores would restrict the permeate flux leading to slower filtration times.

3.1.3 Flow Configuration

There are two common flow configurations for filtration: cross-flow and dead-end. Cross-flow filtration tangentially flows across membrane with some of it flowing across. Dead-end flow is when all the flow is directed through the membrane. Although cross-flow is beneficial due to low blocking from particulates, it increases the amount of dead volume associated with the system as it requires additional interconnections for circulation from the pump. It also increases the amount of time required for filtration as only a small portion of the sample is permeated through the membrane. A dead-end flow system is rapid as the sample is pushed through the membrane. It also has the least dead volume and the elution volume upon backflow is small. Hence, the dead-end method flow configuration was chosen.

3.1.5 Pressure Source

Pressure driven flow source is required for providing the sufficient force to cause permeation of liquid through the pores. There is several ways to apply pressure in a filtration membrane setup. The most common way is using a peristaltic or syringe pump. A peristaltic pump deforms sections of tubing and rotates on a circular wheel to positively displace liquid. A syringe pump pushes fluid out of a syringe using a mechanical motor to control flow. Although both are appropriate for the task, these require electrical power and are not very portable for on-site testing. A manual syringe with a plunger is considered here as a low cost, portable and versatile pressure source for the operation of the filtration unit.

3.1.6 Encasing

The type of material for creating an encasing around our device has the requirement that it not interferes by adsorbing the biological species of interest and be inert. There are a multitude of options that can perform these criteria but Tygon tubing was chosen since it's readily available, durable, cheap, and flexible. Also, interconnects between syringes can be connected to tubing easily without requiring machining or threading. Lastly, tubing sizes can be selected in order to tightly fit a hollow fiber to reduce dead volume. Specifically for 0.2 μm pore size polypropylene hollow fiber with an outer diameter of 2.25 mm, 3.175 mm (1/8") inner diameter Tygon tubing was chosen leaving ~0.5 mm gap between Tygon tubing and outer wall of the hollow fiber.

3.2 Experimental Setup and Method

The final configuration of the device is a single hollow fiber membrane of pore-size with 0.2 μm and length 15 cm, made of polypropylene operating in a dead-end flow mode using only mechanical pumping applied by the user via a syringe. This section details the fabrication of a device, reagents used in the experimental method, sample preparation, and the experimental method itself.

3.2.1 Device Fabrication

As a proof of concept, polypropylene hollow fibers of 0.2 microns pore size were obtained from Accurel Q 3/2 Membrana GmbH and cut into 15 cm segments. The inner diameter was 1.8 mm and wall thickness of 0.45 mm. Arardite two-part epoxy adhesive was used to seal one end of the hollow fiber. The other open end was inserted into a polypropylene female luer

lock/barb obtained from Qosina Corp. and sealed with a combination of Arardite epoxy and Cynergy which is a cyanoacrylate adhesive gel manufactured by ResinLab part of Ellesworth Co. A combination of Cynergy and Arardite were used since Arardite epoxy formed a good bond between the components and Cynergy sealed fiber pores and harden the fiber to stop leaks at the connection interface due to deformation expansion from the membrane. The hollow fiber is threaded into a 1/8" inner diameter Tygon tubing and sealed using Arardite epoxy and connected to another female luer lock/barb.

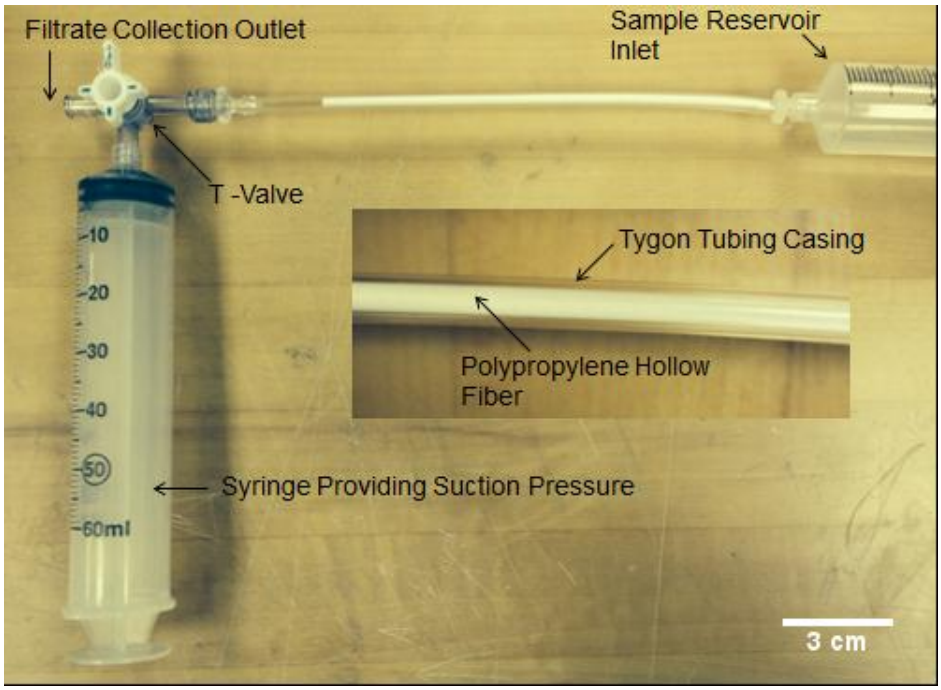

Figure 8: Hollow fiber filtration setup

One end is connected to the space between Tygon tubing walls and shell-side the hollow fiber. Another end is connected to the inside of the hollow fiber. These ends are connected to a T-valve and open 60 ml syringe used as the sample reservoir. Depending on the configuration used during the test, the connection ends can be switched. A closed syringe is added to the T-valve. This syringe added functions to apply negative or positive pressure around the outer space

between the fiber and Tygon tubing or inside the fiber. The device is first sanitized with bleach/water solution and then kept in 70% ethanol solution to keep the device free of bacteria and also to pre-fill the pores of the hollow fiber with solution.

3.2.2 Reagents

Several different reagents must be prepared following standard biosafety standards to avoid contamination. PBS 1x solution (250 ml) is autoclaved as preparation as the filtration solution. Two hundred and fifty ml was chosen mostly due to autoclaving size limitation but it is within the 100 ml to 1L range for extract enough bacteria. LB-Agar plates are made using 1000 ml of DI water and 2:1:2:3 ratio of tryptone, yeast extract, NaCl, and bacterial grade Agar. The solution is autoclaved under a wet cycle at 120°C for 20 mins and set to cool on a magnetic stirrer for 20 mins as temperature reaches ~50-60°C. Five hundred µl of 100 µg/µl stock ampicillin is added which amounts to 50 µg/ml plate concentration. The addition of ampicillin is necessary to reduce the possibility of other bacterial contaminants growing on the plates since the *E.coli* strain used is ampicillin resistant and also facilitate growth of the ampicillin resistant *E.coli* since it is not possible to grow without ampicillin when modified to be resistant. The *E.coli* containing L4440 vector, typically used in *C. elegans* nematodes feeding, are used in these experiments since it was the most abundant, well-studied, and controlled with the facilities available. Three ml of *E.coli* saturated liquid stock is grown in LB medium with 1.5 µl stock ampicillin in a 10 ml culture tube and kept at 4°C. The stock solution is re-inoculated for 18h in new solution every week to ensure viability of *E.coli*.

3.2.3 Sample Preparation

One hundred microliters of saturated *E.coli* stock is inoculated into 3 ml solution in a culture tube and incubated at 37°C in at shaker (Max Q Mix 400 Shaker) for approximately 3 hours. The optical density of the *E.coli* is then measured using a UV-Vis spectrometer (Ultrospec 2100 Pro). The incubation is halted by removing the tube from the shaker when the optical density reaches 0.6 OD. The optical density uses LB medium filled cuvette as a baseline. Optical density of 0.6 indicates that the bacteria are in the middle of exponential growth phase and around ~10^8 cells. This was verified by measuring the growth of bacteria every 30 mins.

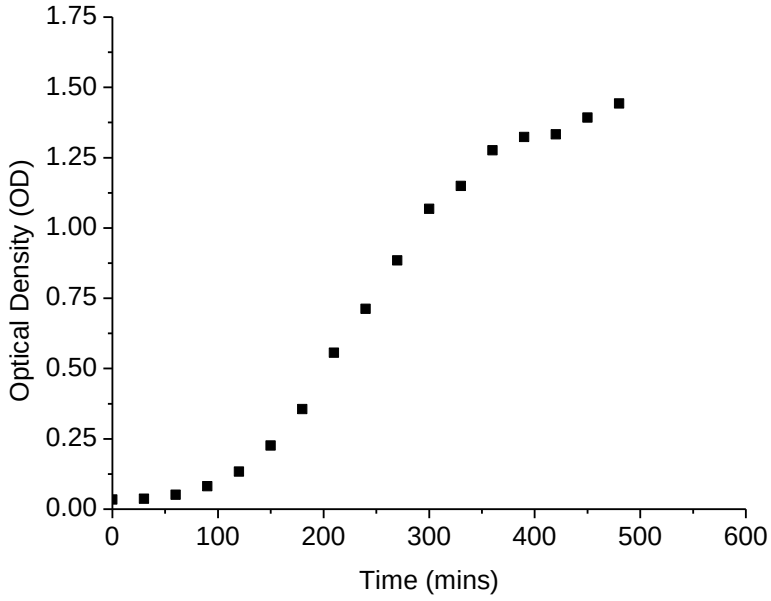

Figure 9: Optical density readings of *E.coli* L4440 using 600 nm wavelength absorbance

One milliliter of solution is transferred to a 2 ml Eppendorf tube and centrifuged at 7000 rpm for 8 mins (Eppendorf Centrifuge 5414D) to concentrate the bacteria into a pellet at the bottom of the tube . The supernatant in the Eppendorf tube is replaced with 1 ml of PBS 1x solution carefully. The medium replacement is done to stop the growth of the bacteria and to suspend it in solution while maintaining bacterial viability. Once the cell concentrate of *E.coli*

in PBS has been made, the initial concentration was determined through cell plating. The dense concentration of cells was diluted in order to be plated and counted as shown in Figure 10. A serial dilution of 100x of the solution was performed three times in succession and plated on the LB-Agar plates to determine the total starting concentration of cells. An extra dilution is made in between the second and third dilution using a 10x dilution as a safeguard in case the cell concentrates is lower than normal. The entire serial dilution process is repeated three times to ensure correct starting cell concentration is correct.

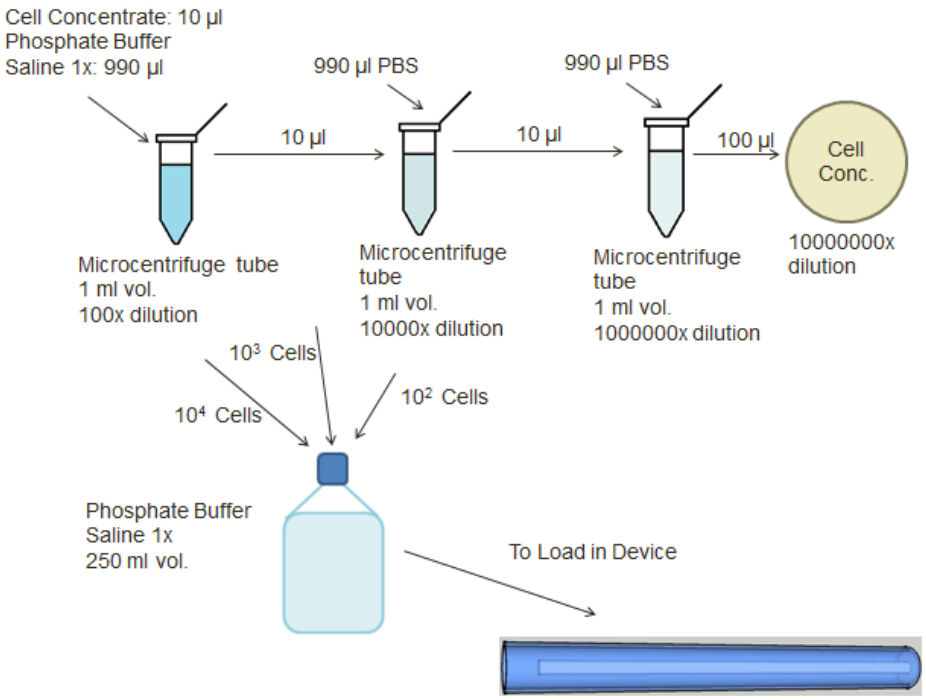

Figure 10: Diagram of serial dilutions and cell seeding

Of the serial dilutions made, a certain concentration of bacteria is selected to be seeded to the 250 ml PBS 1x solution and swirled gently to disperse the bacteria in the container. This solution with varying bacteria concentrations is used as the model sample solution. The hollow fiber filtration device is then prepared for filtration by flushing the 70% ethanol/water solution out using PBS 1x solution several times to ensure all ethanol is removed.

3.2.4 Experimental Setup

The schematic in Figure 11 describes the sequence of steps for the operation of this device. First, the sample reservoir is filled with 60 ml of *E.coli* bacteria/PBS solution and suction is applied Figure 11 a). Suction was found to be better than positive pressure as it caused minimal leakage in the shell-side of the hollow fiber. Furthermore, suction pressure results in a more uniform flux along the hollow fiber compared to positive pressure applied inside the hollow fiber. Positive pressure drives the flow which causes pressure gradient between and the beginning of the fiber and the end of the fiber. Suction pressure has minimal pressure differences at both ends of the fiber and can easily pull the flow inside the fiber and along through the pores uniformly. The average suction pressure applied with a 60 ml syringe was 70-100 kPa as measured using a pressure sensor.

Once the sample reservoir is filled with filtrate due to the applied suction, the T-valve is switched to direct flow to a beaker where the filtrate is emptied seen in Figure 11 b). Once the reservoir is emptied from filtration shown in Figure 11 c), the sample reservoir is filled again with the PBS 1x seeded solution and repeated until the 250 ml is filtered completely.

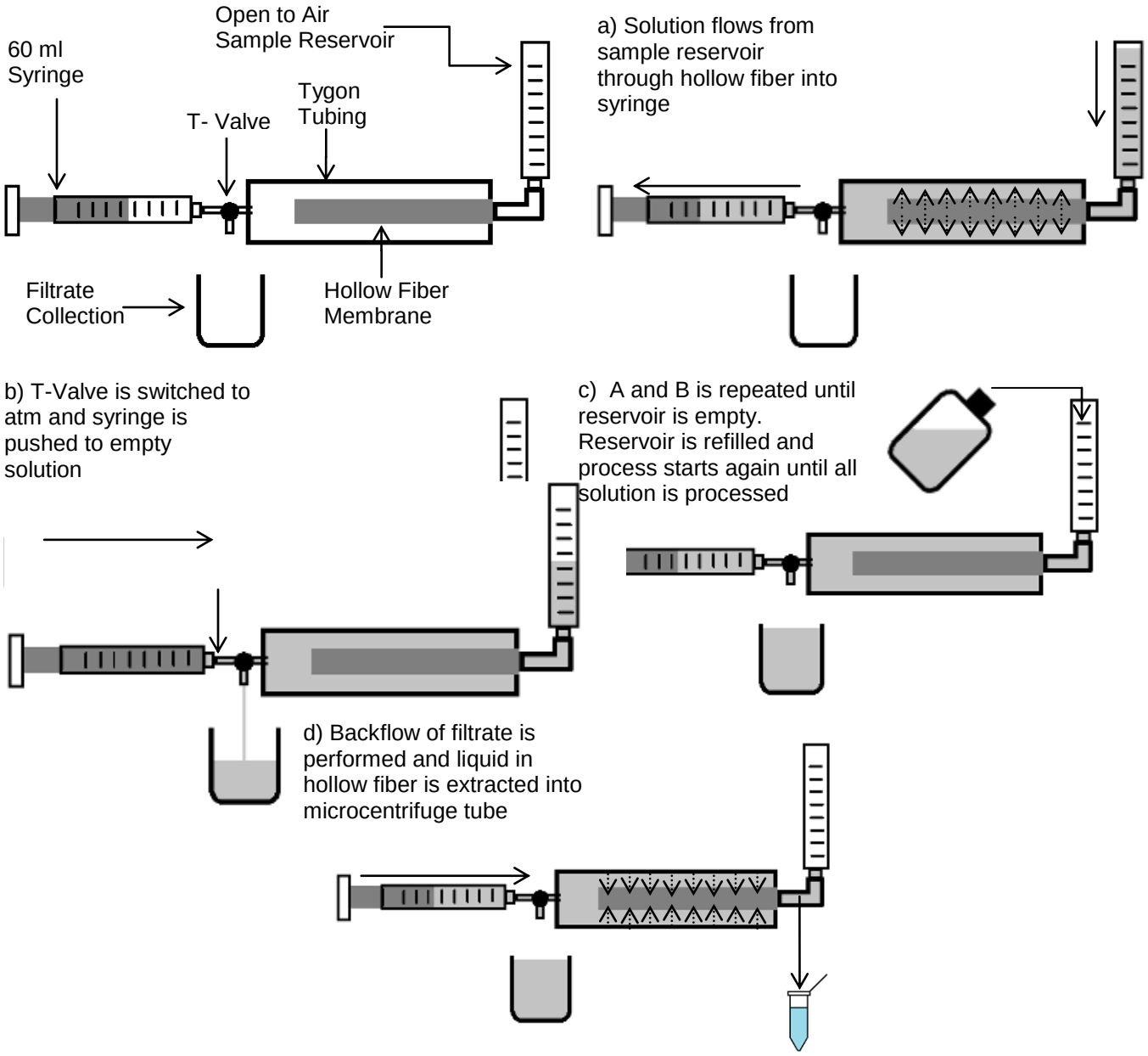

Figure 11: Schematic diagram of solution flow during experiment

The filtrate is the solution that has passed through the membrane and collected in the beaker and syringe. The retentate is defined as the remaining concentrated bacterial solution within the hollow fiber device. The location of the retentate is dependent on the device configuration since two different configurations were initially used as shown in Figure 12. The configuration in Figure 12 a) uses the inner surface of the hollow fiber (flow inside out) as the membrane (lumen-side), and the configuration in Figure 12 b) uses the outer surface of the hollow fiber (flow outside in) as the membrane (shell-side). Both lumen-side and shell-side filtration modes were tested during the preliminary stages to determine the more optimal mode. For both setups, at least 1 ml of the filtrate is back flushed to wash off the retained bacteria concentrated on the hollow fiber which is collected in a 2 ml eppendorf tube. This retentate is plated directly or serially diluted depending on the possible concentration of cells. All plates are repeated three times to prevent plating error.

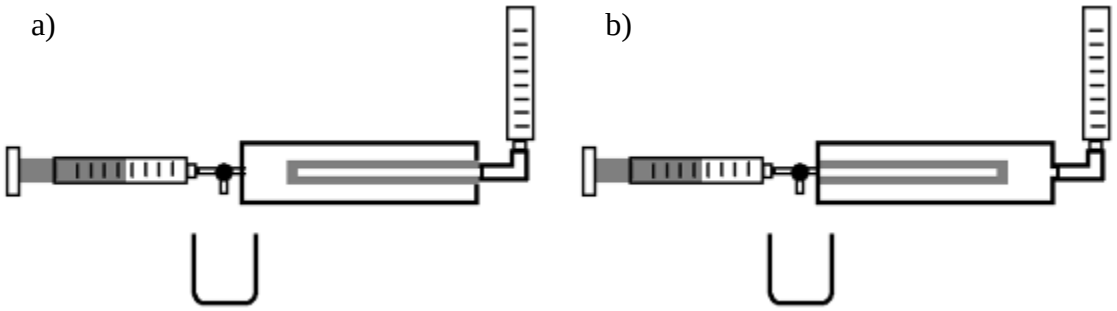

Figure 12: (a) Lumen-side membrane configuration and (b) shell-side membrane configuration

3.2.5 Fiber Length Determination

The amount of dead volume associated with filtration is directly related to the length of the hollow fiber. Since the hollow fiber inner diameter is 1.8 mm, the calculated cross-sectional area is 0.0254 cm^2. Thus, the dead volume increases with length about factor of 0.0254 ml/cm.

$$Dead\ Volume = 0.0254 \frac{ml}{cm} * Length\ of\ Fiber$$

Although it is beneficial to have shorter fibers to minimize the dead volume, the flux through the membrane as well as its capacity will also be reduced. The flow rate is directly related to surface area of the hollow fiber. For water samples, the flow rate is 2 ml/(hr cm^2 kPa) calculated from Section 3.4.2 which leads to a flow rate of 1.13 ml/hr kPa per 1 cm of length.

$$\frac{Volume}{Length\ of\ Fiber * Pressure * 1.13 \frac{ml}{hr\ kPa\ cm}} = Time$$

Assuming that a typical pressure of 85 kPa (70-100 kPa average suction pressure from 60 ml syringe) is applied to a 250 ml sample, a fiber length of ~15 cm is required so that the filtration can be performed under 10 min. The specification noted are based on the operation of the hollow fiber device in experimentation

The calculated dead volume for 15 cm length is 0.4 ml. However, several times (5-6) that dead volume of 0.4 ml should be eluted back to ensure adequate resuspension of the retained bacteria.

3.3 Results and Discussion

The ultrafiltration membrane that is used is asymmetric with small pores on one side and large pores of the backing on the other side. In order to test the filtration efficiency and its dependence on the flow direction across the membrane, two designs shown in Figure 12 were tested. In the design shown in Figure 12 a), the flow of the sample was from the lumen out to the shell side. In this configuration, the sample encounters the smaller pore sizes on the lumen side which retains the bacteria. In the design shown in Figure 12 b), the flow of the sample was from

the shell side into the lumen. The sample approaches membrane on the side that has large pores which narrow down to smaller pore sizes as it reaches the lumen. The pore size on the shell side is large than the bacteria while that on the lumen side is smaller.

The Figure 12 b) setup was initially tested with two different volumes of 10 ml to test an initial proof of concept and a larger 250 ml of volume as a simulation of a typical contaminated sample, both with 10^5 bacterial cell in that volume. The goal was to incrementally reduce the bacterial concentration in the sample and eventually to test samples with very low amounts of seeded bacteria to mimic drinking water concentrations.

In an ideal filtration operation, all the cells in the initial sample are retained and extracted as retentate and none pass through the membrane into the filtrate. Therefore, the CFU counts of the sample and the retentate should be nearly the same while the count in the filtrate should be zero. The amount of cells seeded into the test is calculated by determining the initial cell concentration via cell counting and determining the dilution factor. Table 2 contains data from the hollow fiber shell side filtration experiments. The elution volume is the final volume extracted from the device after the filtration process was completed including the backflow flushing volume. Seeded bacteria is the amount of bacteria added to the sample solution which is determined by plate counting the cell concentrate, multiplying by the dilution factor used during seeding, and volume added to 250 ml or 10 ml solution. The retentate average is determine in the same process of plate counting the retentate plates, multiplying by the dilution factor if used, and amount of elution volume for the amount of bacteria found. The standard deviations associated with each experiment are from CFU count of the plates. Recovery represented in Figure 13 is the retentate average divided by the total amount of seeded bacteria.

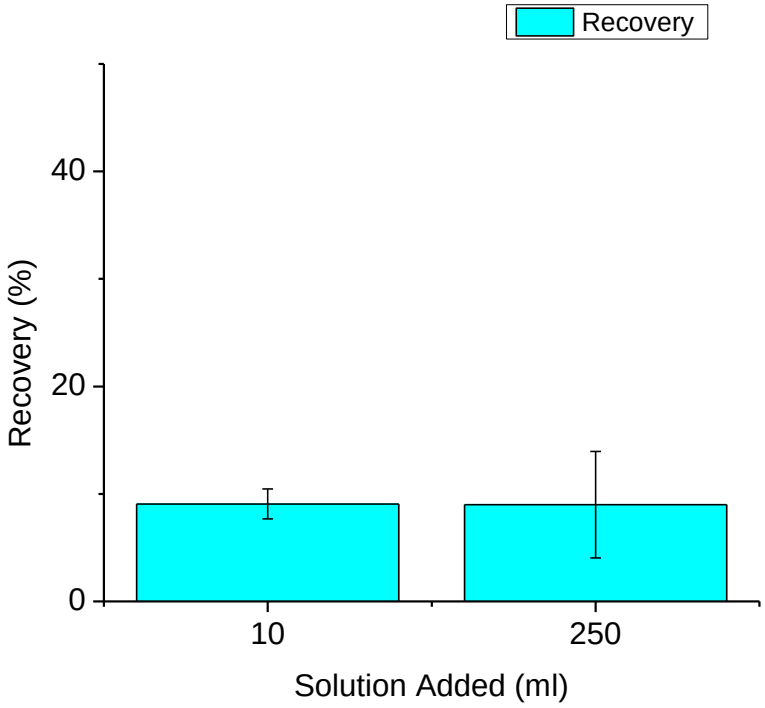

Figure 13: Recovery of hollow fiber shell-side pre-concentration experiments

Table 2: Two proof-of-concept shell-side hollow fiber filtration with 10 ml seeded solution and 250 ml seeded solution

	10 ml Solution	**Standard Deviation**	**250 ml Solution**	**Standard Deviation**
Elution Volume (ml)	1.0		2.5	
Seeded Bacteria	1.9×10^5	2.6×10^4	1.3×10^5	6.5×10^4
Retentate Average	1.2×10^4	1.0×10^3	1.2×10^4	3.0×10^3
Filtrate Average	0	0	0	0
Recovery	16%	2.5%	16%	5%

Figure 13 shows a significantly low concentration of the seeded bacteria in the eluted volume. In both experiments, a ten times reduction in recovered bacteria (~10% efficiency) compared to the initial seeded bacteria. Furthermore, no cell counts was detected in the filtrate even at 1.9×10^5 seeded bacteria concentrations concluding that the shell side of the membrane of the hollow fiber was retaining most of the bacteria even after multiple back flush.

This is likely to occur since SEM reveals the shell side of the membrane has large pore sizes and decreases in size as it approaches the lumen side of the hollow fiber. Therefore, the possibility of internal fouling and build up is larger on the shell side rather than the lumen side. A comparison of the topographical features of two sides of the membrane is shown in Figure 14 at the same 1333x magnification. It is very apparent in Figure 14 a) that the lumen side of the membrane should be the filtration side since the pores are closest to 0.2 μm and thus only lumen membrane filtration was experimented further on.

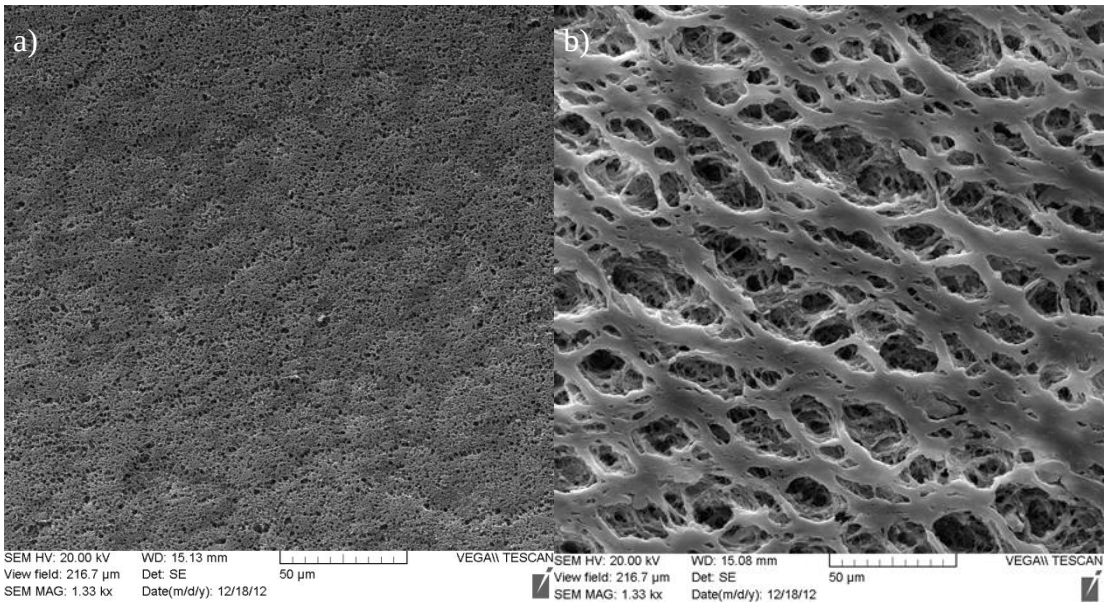

Figure 14: (a) Lumen side of polypropylene hollow fiber membrane 0.2 μm pore size (b) shell side of same hollow fiber

Subsequently, the design Figure 12 a) was tested which uses the lumen-side of the membrane. Filtrations have been done on 250 ml samples with 3.0×10^4, 2.2×10^3 and 2.4×10^2 bacteria seeded in them. Elution volumes were 2.50 ml, 2.51 ml, 1.52 ml respectively measured by scale and by pipette.

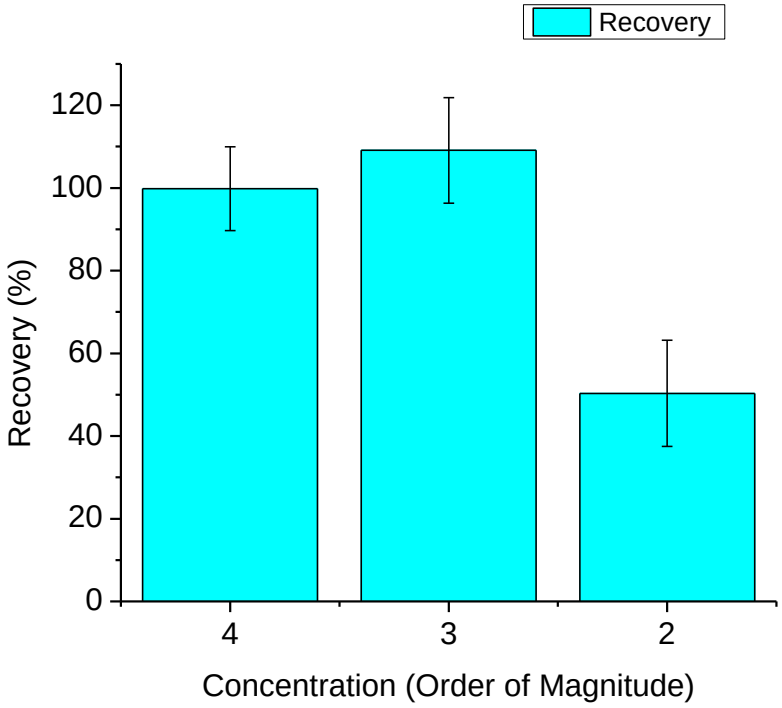

Figure 15: Recovery of hollow fiber pre-concentration lumen side experiments

Table 3: Plate count results for hollow fiber from pre-concentration experiments

	10^4 Experiment	**Standard Deviation**	**10^3 Experiment**	**Standard Deviation**	**10^2 Experiment**	**Standard Deviation**
Elution Volumes (ml)	2.50		2.51		1.52	
Seeded Cells	3.0×10^4	3.2×10^3	2.2×10^3	1.3×10^2	2.4×10^2	4.1×10^1
Retentate Count	3.0×10^4	1.0×10^3	2.4×10^3	2.6×10^2	1.0×10^2	2.3×10^1
Filtrate Count	0	0	0	0	0	0
Recovery	100%	10%	109%	13%	50%	13%

For experiments with 3.0×10^4 in 250 ml, the recovery is consistently around 100%. The 2.2×10^3 bacteria seeded experiment achieved 109% recovery which it is impossible to recover more than the bacteria seeded. It is most likely the recovered amount is 100% and higher than normal counts were recorded of the three plate counts. The plate count standard deviation associate with this result makes it within the 100% range. Moreover, the amount of significant figures associated with plate counting is 2 resulting in 10% standard error [33].

Total retention is expected as the pore size is smaller than the bacteria preventing its passage through the membrane. However, at low amounts of seeded bacteria (~240 bacteria cells), there is a significant drop in recovery (~50 %) without any detectable bacteria in the filtrate meaning all the bacteria is retained but not all the bacteria was recovered. This drop in recovery may be related to the limitations of cell plating technique and the precision in counting associated with it. The amount of countable colonies in the seeded plates in 240 seeded bacteria test is under 10. Colony counts under 10 per plate are well below standard limits for microbiological counting of water [33]. The other reason could be that the bacteria adhere to the walls or cavities of the pores and are difficult to dislodge similar to the shell-side experiment i.e. membrane fouling. The backflow strength might not have been enough to produce strong enough force to remove the bacteria from the membrane walls. The flow rate of 1.45 L/hr is calculated from Section 3.3.1 with 85 kPa pressure with 15 cm. The backflow seemed to work for 3.0×10^4 and 2.2×10^3 cells, but the result could be false since the majority of bacteria remaining on the hollow fiber could be much lower than the standard deviation. In 240 seeded bacteria case, this effect would be more prominent as most bacteria would be adhered to the wall instead of suspended in solution. Membrane fouling is a well-documented phenomenon which cannot be avoided but only mitigated [34], [35], [36], [37].

3.3.1 Flow Rates and Permeation Time

The amount of time on average for filtration varied depending mostly pore permeation. On average, 250 ml of solution would permeate through the hollow fiber within 10-20 mins if all pores are open. If some pores were air-filled or blocked due to contamination from particle contamination, the time of filtration increases significantly.

Flow rates can be calculated using the pore flow model. According the pore flow model, the permeate flux for solvent is related to pore diameter and the pressure drop across it according to equation (1) [28]:

$$J_v = \frac{\varepsilon_m d_p{}^2 \Delta P}{32 \mu l_p} \tag{1}$$

in which J_v is permeate flux in volume/(time*area), ΔP is transmembrane pressure, ε_m is porosity, d_p is average pore diameter, μ is viscosity, and l_p is average pore length. The above equation can be simplified to a form with R_m as the flow resistance

$$J_v = \frac{\Delta P}{R_m} \tag{2}$$

The model only incorporates the resistance of the membrane with the solvent and does not include solute. Other resistances such as a cake layer build up due to fouling; concentration polarization and reverse osmotic pressure is usually included in this model as

$$J_v = \frac{\Delta P - \Delta \pi}{R_m + R_c} \tag{3}$$

where π is the reverse osmosis pressure and R_c is hydraulic resistance due to filter cake and gel layer. Reverse osmosis pressure is due to a buildup of salt and ions at the surface of the membrane causing a localized concentration gradient across the membrane which leads to a pressure generation. Since the pressure is 70-100 kPa and the pores are 0.2 μm which is fairly large compared to salt and ions, the salt easily passes through the pores without much hindrance, resulting in little to no build up. Thus, the reverse osmosis effect is negligible compared to the pressure applied. The filter cake hydraulic resistance (R_c) from bacteria adhesion, pore blocking

and build up is another factor in membrane resistance. The filter cake hydraulic resistance (R_c) value can also be assumed to be very low, but not negligible for water filtration since it is assumed very low amounts of bacteria exist in drinking water. The hydraulic resistance does increase slowly as experiment continues as more bacteria accumulates on the surface creating a layer of bacteria. The hydraulic resistance increases since the flow must pass through an addition layer of bacteria. The flow rate can be calculated based on this model.

An experiment to find the flow conductance ($1/R_m$) value was performed using 15 cm length hollow fiber to stay consistent with actual device usage. Based on equation (2), the flow hydraulic resistance can be found by keeping the flow rate (J_v) constant via syringe pump and measuring the pressure difference (ΔP) at steady state (~ 20 mins) seen in Figure 16. By changing the flow rates and measuring the pressure, flow conductance ($1/R_m$) value is determined by calculating the slope of the curve. A linear interpolation is performed on Figure 16 using y = bx where y is the flow rate, b is flow conductance ($1/R_m$), and x is pressure. Flow resistance (R_m) was determined as 17 ml/(hr kPa) with $R^2 = 0.994$.

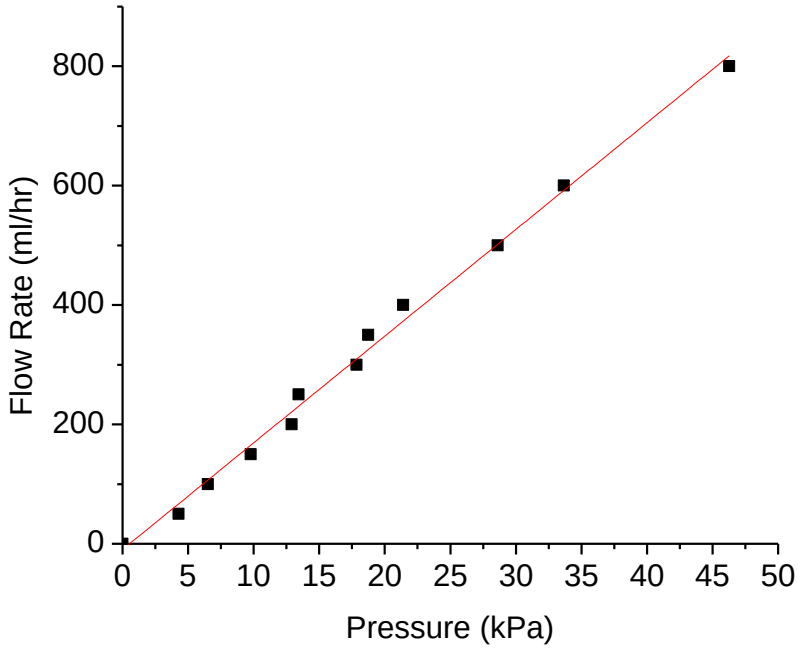

Figure 16: Pressure measurement with varying flow rates with dead end flow 15 cm polypropylene hollow fiber

The hollow fibers used here are 15 cm in length and with an inner radius of 0.9 mm. The total inner surface area of the fiber is 15 x 2 x 0.09 x π = 8.5 cm^2. Using flow resistance (R_m) determined 17 ml/(hr kPa) and the surface area of inside of the hollow fiber, the flow rate per unit area and pressure is 2 ml/(hr kPa cm^2) which is comparable to that provided in the hollow fiber technical data sheet for isopropanol (>1.2 ml/(hr kPa cm^2 at 25°C)). The average pressure exerted by hand with 60 ml syringe was measured at 70-100 kPa which suggests that it would take ~ 10 min to filter 250 ml. The amount of pressure applied can be increased by creating a device that fits with a syringe, such as a crank, to provide a mechanical advantage instead of operating by hand. The maximum amount that can be applied though would be 4 bar or 400 kPa beyond which the hollow fiber can implode or collapse according to its data sheet.

3.4 Summary

A simple hollow fiber based device can successfully reduce 250 ml volumes water and retain bacteria in relatively short period of times (10-20 mins) which the focus is to replace the conventional incubation and transporting. Although conventional incubation does provide the higher concentrations, incubation is 18-24 hours to complete. A primary advantage to this process is that it is directly related to the amount of pressure used and the amount of hollow fiber in each module can be tailored to optimize the filtration time and flow rates. Although all tests done for ~10^2 bacteria (~240 seeded bacteria) produced lower recovery, it is not clear if they are retained on the membrane or in the rest of the device.

The limits to this hollow fiber are the amount of dead volume in the 1-2 ml range and that biofouling can occur. Since the eluting volume from this device is 1-2 ml, it is too large to pass directly to a microfluidic device. Thus, another filtration phase will be introduced within the microfluidic device as a preprocessing step to further reduce the volume to ~ 5 μl.

Chapter 4 Microfluidic Sample Filtration Device

This chapter details the design, fabrication and preliminary testing of a microfluidic filtration device that is capable of reducing samples from ml to µl. It details the choice of materials for fabrication of the microfluidic device followed by various bonding methods used in microfluidic devices. A new bonding method to bond ultrafiltration membranes with PDMS is developed and the bonding characteristics tested.

4.1 Filtration Techniques in Microfluidic Devices

All microfluidic devices that process field samples require some form of sample preparation. Separation or filtration is a critical element of this sample preparation. Many different separation and filtration processes have been developed in the recent years for miniaturized total analysis system. They can be categorized into four major groups, (1) Hydrodynamic Filtration, (2) Ratchet Based Filtration, (3) Electrical Force Fractionalization and (4) Membrane Filtration.

4.1.1 Hydrodynamic Filtration

Hydrodynamic filtration utilizes the laminar flow profile in microfluidic channels and clever channel design to separate different particulates based on size. One example of this technique is pinched flow fractionalization demonstrated by Takagi and Yamada in Figure 17 where two inlets, one carrying particles of two sizes and the other carrying buffer solution at a higher flow rate, meets at an pinched intersection [38]. The fast buffer solution flow squeezes the sample fluid to the channel wall. In the pinched intersection, the larger particle has a greater chance of interacting with the faster buffer flow and therefore gains a greater momentum and

moves to the center of the channel. As the flow widens to a large channel, the large particulates continue near the middle of the large channel and the smaller particulates remain close to the wall of the channel and are carried away to different branches.

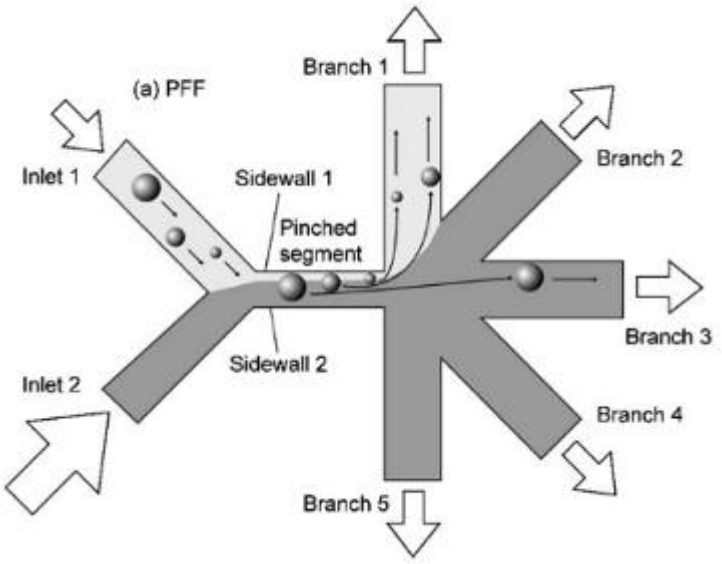

Figure 17: Pinched flow fractionalization with five outflows [38]

Similar to this concept, another continuous flow method by M. Yamada and M. Seki uses a straight channel carrying multiple micro beads with multiple perpendicular outlet channels essentially acting as multiple pinched flow fractionalizations has also been implemented [39]. The multiple outlets because the smaller particles to eventually align on the outer edge of the main carrier channel while the large particle remain in the middle similar to the previous example. Eventually, small particles enter the perpendicular outlets first while the larger particles eventually flow out in the main channel as they are farther away from the edge wall. In both of these devices, the particles in the size range of 0.5 μm – 3 μm can be separated with a high throughput of 100, 000 particles per hour. However, some of the smaller particles are still trapped in the main channel and therefore the efficiency of this method is low. For instance,

~40% of the 2.1 μm and 3.0 μm particles are not separated and still flow out of the main channel. In addition, these devices require an exact flow rate to be set, which may be difficult in field applications.

4.1.2 Ratchet Based Filtration

Ratchet based filtration uses methods that require the particles to separate as they travel through and interact with asymmetric or constraining structures in the fluid flow. Mainly, fluids are passed through asymmetric designed arrays to allow large particles to flow medially and smaller particles to move laterally. There are two main classes in ratchet based filtration (1) Brownian Motion and (2) Lateral Displacement

4.1.2.1 Brownian Ratchet

Brownian Ratchet is essentially using Brownian motion or natural diffusion to separate particulates. Huang, L. *et. al.* [40] demonstrated an Brownian ratchet design by diagonally displaced rectangular pillars optimized to separate three different DNA base pair lengths. Due to the natural Brownian motion and flow, the smaller DNA diffused laterally to path two in Figure 18 while the larger DNA did not diffuse as much and remained in path one. This operation performed over a number of these structures will eventually separate out DNA of different lengths from each other.

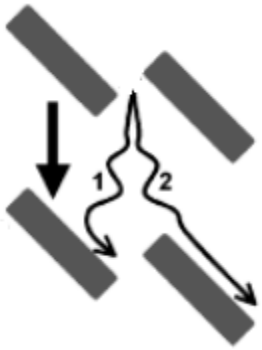

Figure 18: DNA ratchet design field flow fractionalization [40]

Although this method is suitable for DNA, it will not be suitable for larger particles as the difference in Brownian displacement is not large enough. Furthermore, slower flow rates must be used in order to allow time for diffusion to occur, making this a low throughput process.

4.1.2.2 Deterministic Lateral Displacement

Deterministic Lateral Displacement design is based on shifted posts laterally in each row to create stagnation points [41] and is shown in Figure 19. Small particles represented in red in Figure 19 are much smaller than the gaps between posts and therefore the posts do not impede their flow. Larger particles represented in green are of the same size as the gap between posts and therefore hit stagnation points which can shift the particle into another flow stream. Thus, the particle is "laterally displaced". This operation performed over a number of times will lead to a spatial separation of one type of particle from another. The efficiency of this design has been improved by using triangular post shapes [42].

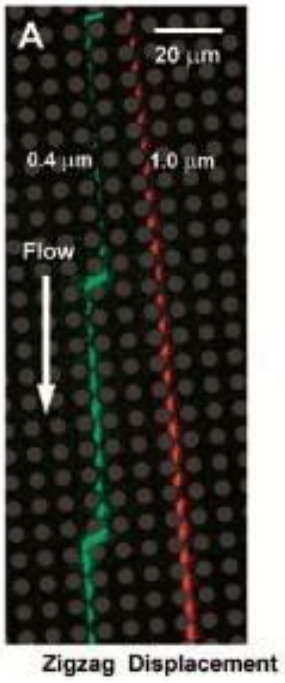

Figure 19: Deterministic lateral displacement array with 0.4 μm and 1.0 μm fluorescent bead [41]

The size range for this separation technique is up to 1 μm size with resolution of 0.1 μm separation at 400 μm/s. The disadvantage to this method is that it is prone to clogging and only very specific sizes can be isolated from a design point of view. It is not suitable for smaller particle sizes as well.

4.1.3 Electrical Force Fractionalization

To enhance the separation efficiency, the use of many kinds of external forces such as magnetic [43], [44], [45], thermal [46], [47], acoustic [48], [49], [50], and optical [51], [52] have been investigated. Most of these techniques are quite established and are mainly for trapping particles. The disadvantages are a requirement of binding substrate or a requirement of additional equipment for the application of external forces. Electrical forces have been of considerable interest in this context as they are easier to integrate in microfluidic device as

compared with other forces. There are two electrical forces used in particle separation which are (1) electrophoretic force and (2) dielectrophoretic force

4.1.3.1 Electrophoresis

Electrophoresis moves charged particles in a fluid through a separation matrix by applying an electric field. It is typically used to separate macromolecules such as DNA and proteins in gel matrix. A version of this technique known as free flow electrophoresis (FFE) is employed to separate larger particulates and cells in free solution in a microfluidic device. The first to demonstrate electrophoresis using beads in a silicon microfluidic chip was D. Raymond *et. al.* [53], and the technique came to be known as free flow electrophoresis. Since then, a myriad of FFE techniques on various substrates and using a number of electrode designs have been integrated into microfluidic chips [54], [55], [56], [57], [58]. The flow rates and electric field strength vary depending on the channel designs and volumes. These chips have been used to separate proteins and to a lesser extent cells. In addition to the complexity of the design and its fabrication, there are also problems associated with bubble formation, long residence times, and joule heating.

4.1.3.2 Dielectrophoresis

Dielectrophoresis is the transport of a polarizable particle in a non-uniform or gradient electric field. Dielectrophoresis is different from electrophoresis in that the analytes must only be polarizable instead of being charged, and a gradient electric field is required. A well-known technique using dielectrophoresis is the split thin flow fractionalization technique method (SPLITT) which implements the use of dielectrophoretic force to separate sizes [59], [60], [61]. An H-channel is used where a non-uniform external electric field is applied perpendicular to the

channel using different varying electrodes [62]. This causes a dielectrophoretic force vertically causing larger particles to be forced downwards.

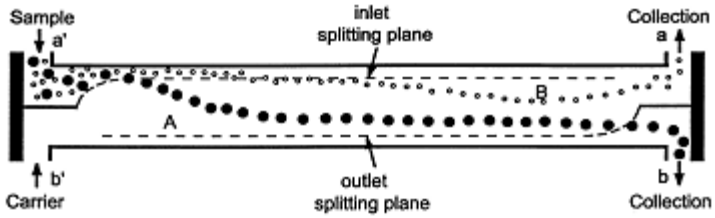

Figure 20: SPLITT diagram setup [56]

The major disadvantage of dielectrophoresis is that most particles are required to be of the same polarizability in order to have the same separation force relative to size. The method has been shown to work with 5 μm beads up to 100 μm beads. Another case separated 1 μm beads efficiently using 500 μm/s flow rates using 20 V [63]. The size range and flow rate are dependent on channel and electrode design.

4.1.4 Membrane Filtration

Membrane filtration in microfluidic devices is a well-known and common method [64]. Membranes separate by impeding the further movement of target particulates larger than their pore size through them while allowing the smaller particles and the solvent through. In order to incorporate a membrane into a microfluidic device, it has to be bonded between two channels, typically top and bottom, in either cross-flow or dead-end configuration. Furthermore, a membrane retains 100% of bacteria from size exclusion which is most important since very few bacteria exist in water solution, and a maximum sample size must be transferred to the next section. Understandably, there are problems with biofouling associated with membrane techniques which can be mitigated by the choice of material used in the membrane. Furthermore, the transmembrane pressure must be lower than the bonding strength of the

microfluidic device for permeation to occur. Currently, very thin nanoporous polycarbonate membranes [65], [66] or anodized alumina membrane [67], [68], [69] have been successfully integrated with microfluidic channels [70]. But, these membranes are expensive as compared to commercially available ultrafiltration membranes and microfiltration membranes. If commercial membranes can be used, it would provide greater flexibility in the choice of membrane types and pore sizes

4.1.5 Summary of Filtration Techniques within Microfluidic Devices

Although, most of the filtration methods mentioned above have their own advantages and disadvantages, membrane filtration is only one technique that satisfies the most important factor which is retaining the entire bacteria sample. It is also fairly simple and straightforward and hence is expected to be easy to operate. The other disadvantages such as biofouling or bond strength can be alleviated through incorporating possible solutions in the design phase.

Table 4: Summary of microfluidic filtration methods

Method	Advantages	Disadvantages
Hydrodynamic Filtration	-Able to be selective in terms of size -Requires no filter, limited biofouling	-Low yield -Sensitive to flows and pressure -Requires secondary flows or multiple outlet control
Ratchet Based Filtration	-Requires no filter -Good for smaller particles for diffusion -Fast flow rates (Lateral)	-Low yield -Sensitive to flows and pressure -Irreversible blocking -Requires secondary flows or multiple outlet control
Electrical Force Fractionalization	-Easy addition with Hydrodynamic Filtration -Good size separation -Flow rates tunable to design	-Dependent on particle charge or polarizability -Requires secondary flows or multiple outlet control -Joule heating or bubble formation -Additional power source
Membrane Filtration	-100% retention of bacteria -Available for all ranges depending on filter	-Biofouling -Require resistance to pressure (bond strength)

4.2 Materials Used in Microfluidic Device

Investigation into the suitable types of materials for membrane filtration is detailed in this section. Also, the method of bonding the membrane with the microchannels is discussed.

4.2.1 Membrane Material

An important aspect of the choice of a membrane to integrate within a microfluidic device is the compatibility of the material type to bonding. There are several materials to choose from in terms of membrane type aforementioned in the hollow fibers section. The most common choice is nanoporous polycarbonate membrane due to easy integration [60], [61], [62], but polycarbonate has very low pore density and is expensive since the pores are usually physically etched via RIE. Integration of non-typical membranes for microfluidic devices were considered since commercial ultrafiltration membrane types will provide higher pore density, larger variety, and lower cost. In this matter, commercial modified flat sheet polyethersulfone membranes (OMEGA Pall) are of particular interest because of their low and reversible fouling as well as the strong structural support that they provide due to polyolefin backing. The reduction of biofouling greatly reduces the amount of possible loss of bacteria during back flush and increases device lifetime.

The pore size of the membrane is chosen to be much smaller compared to the bacteria such that the bacterial cells do not get embedded in the pores and biofoul. Although smaller pore size produces smaller throughput, this tradeoff is acceptable considering that this second stage filtration only processes approximately 1-2 ml of pre-concentrated sample that comes from the first stage hollow fiber pre-concentration filtration. Among the various configurations possible, the flat sheet configuration is the easiest to integrate with a microfluidic channel through the

"sandwiching" method [70]. A commercial asymmetric polyethersulfone membrane (Pall OMEGA Membranes) was selected seen in Figure 21; created through wet inversion emulsion techniques. OMEGA ultrafiltration PES membrane was used from Pall at 10 kDa and 70 kDa pore size.

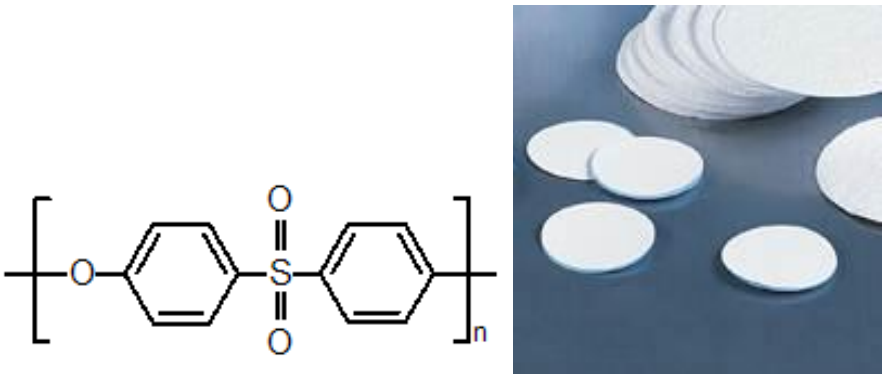

Figure 21: (Left) PES polymer repeating chemical structure (Right) Pall OMEGA disk-form PES membranes

4.2.2 Microfluidic Device Material

The most widely used microfluidic material is PDMS as it is easy to prototype microfluidic devices in it rapidly through soft lithography techniques [70], [74]. Other possible materials such as glass and silicon have been used for microfluidic devices but are difficult and more expensive to process. The type of PDMS is a commercial two part (curing agent and base) vinyl-terminated PDMS from Dow Corning (Sylgard 184). The PDMS is made using a 10:1 wt% ratio of base-to-curing agent seen in Figure 22.

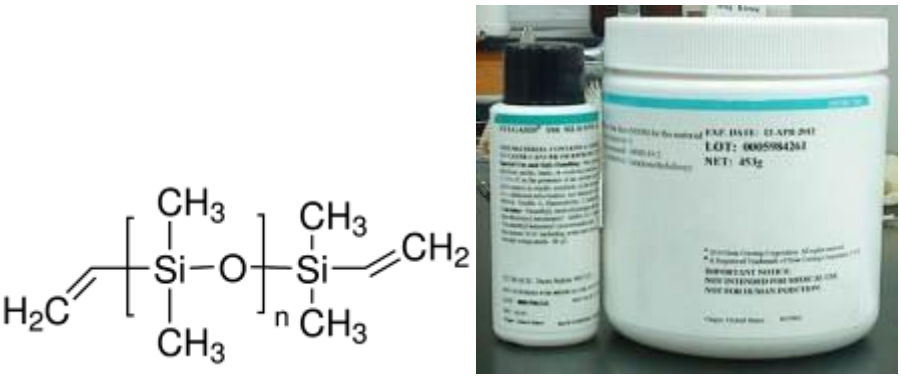

Figure 22: (Left) Uncross linked PDMS polymer repeating structure (Right) purchased two-part vinyl terminated PDMS Sylgard 184

4.3 Membrane Integration Technique

Different membrane methods for integrating flat sheet PES membranes into PDMS were investigated. There are four main ways in literature that were possible for bonding flat-sheet PES membrane with PDMS. They are clamping, direct casting [29], *N*-Methyl-pyrrolidone solvent assisted bonding [75], [76], and bonding using chemical intermediate cross linkers [77]. Each of these methods was used to identify the most reliable method for integration.

Clamping causes deformation of the flexible PDMS microfluidic channel and non-uniform force distribution at the interface. Furthermore, as the membrane surfaces were uneven, there were little crevices that were formed which caused leakages. Therefore, this method was not considered suitable.

Direct casting is also not applicable in our case simply due to the nature of the method. Direct casting is coating the membrane with a very thin layer of PDMS characteristically for pervaporation methods (i.e. ethanol and water separation). Although the method is fairly good for pervaporation application, the blocking of pores is unsuitable for this application.

This *N*-Methyl-pyrrolidone solvent assisted bonding and bonding using chemical intermediate cross linkers as the two most applicable methods for integrating flat sheet PES membranes into PDMS.

4.3.1 N-Methyl-pyrrolidone Solvent Assisted Bonding

N-Methyl-pyrrolidone (NMP) is a dipolar aprotic chemical usually used as a solvent. *N*-Methyl-pyrrolidone solvent assisted bonding was the first proposed by Ye Gu *et. al*. [76] for bonding of PES membrane and PDMS. Ye Gu *et. al*. [76] microcontact printed NMP onto a PES membrane by spinning NMP on a silicon wafer at 1000 rpm and using a PDMS stamp to transfer NMP to PES membrane. A thin film of NMP would be retained by the PDMS when removed from the wafer. Upon contact with PES, NMP would partially dissolve the PES into the PDMS, evaporate and form a good bond. Upon repeated trials, the results reported in the paper were non-replicable in our setting, and the PDMS delaminated easily from the PES membrane. There are several reasons why this method may not be replicable in our case. Firstly, in [31], the PES membrane with 200 μm thickness fabricated in house used very short chain PES (MW 4800) which allowed for better diffusion. In addition, the details about the kind and chain length of PDMS used were also not provided. Therefore, when used with commercially available PDMS and PES membrane with polyolefin backing, this method did not produce the expected results.

More fundamentally, it is not evident that this method would be feasible. A simple comparison of solubility parameter shows a large mismatch (NMP: 11.1 $cal^{1/2}$ $cm^{-3/2}$, PDMS 7.3 $cal^{1/2}$ $cm^{-3/2}$) [78]. Ideally, the parameter has to be similar or close to each other to dissolve. In addition, Ye Gu *et. al.* [76] stated that NMP was evaporated quickly (under an hour) after bonding. It is unclear whether this is possible at low temperatures as the boiling point of NMP is

206.1°C (93rd edition of the CRC Chemistry and Physics Handbook) and high rates of evaporation are possible only near boiling point temperature at which the PES membrane would soften and reflow.

4.3.2 Intermediate Crosslinking Agents

The other method of bonding is using a chemical intermediate cross-linker between PES and PDMS in order to cause two materials to bond. The only cross linker mentioned in literature for PDMS to PES bonding is (3-Aminopropyl)triethoxysilane (APTES) [77] whose chemical structure is shown in Figure 23. APTES cross-linker hydrolyzes at pH 2 transforming the ethyl groups on APTES to hydroxyl groups (-OH). The hydroxyl groups bonds to other materials via amine bond and hydroxyl bond seen in Figure 23.

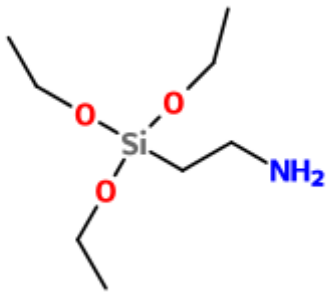

Figure 23: APTES silane chemical composition

According to Aran *et. al.* [77], the APTES is hydrolyzed in water at 80°C at 5% concentration by volume.

$$\text{APTES} + \text{Water} \xrightarrow{80C} \text{Hydrolyzed APTES} + \text{Ethanol}$$

The hydroxyl end group of APTES is bonded to the PES membrane after air or oxygen plasma oxidation of the surface which introduces hydroxyl groups. Subsequent soaking in 5% APTES solution leads to APTES capped PES membrane.

$$\text{PES Membrane} \xrightarrow{\text{Plasma Oxd}} \text{PES Membrane-OH}$$

$$\text{PES Membrane-OH} + \text{Hydrolyzed APTES} \rightarrow \text{PES Membrane-O- APTES}$$

Then, the material is then air dried and bonded to PDMS which has also been plasma oxidized to introduce OH groups on the surface via amine groups on APTES.

$$\text{PDMS} \xrightarrow{\text{Plasma Oxd}} \text{PDMS-OH}$$

$$\text{Hydrolyzed APTES } -(CH_2)_3\text{-}NH_2 + \text{PDMS-OH} \rightarrow \text{APTES-}(CH_2)_3\text{-NH-PDMS}$$

A weight is applied during the bonding process to achieve good contact between membrane and PDMS

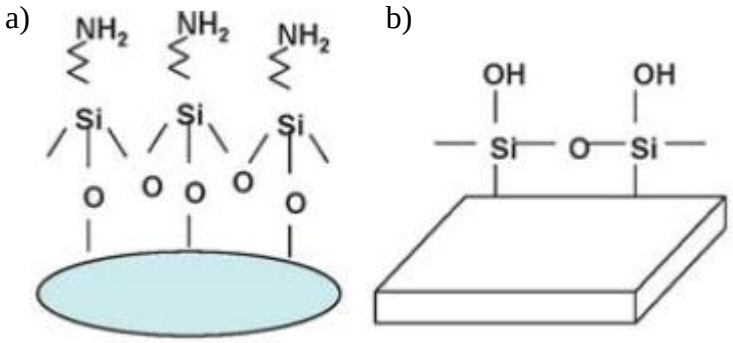

Figure 24: (a) APTES bonded to PES membrane via hydroxyl bond fortified with plasma oxygen (b) PDMS treated with plasma oxygen to expose hydroxyl groups. The two materials are connected by amine bond. [77]

Aran *et. al.* [77] initially performed bonding of PCTE and PES. When replicated, PCTE membrane bonding process works extremely well achieving bonding results that cause the

membrane to break into smaller pieces or cause the PDMS to break apart indicating strong irreversible bonding. Unfortunately, when the same process was used to bond PES with PDMS, the bonding strength was weak. Although there is some bonding, the bond strength was quite low at 24 kPa quantified by burst test described in Section 4.6.2. It speculated that the pore size of the membrane may have caused a difference in bonding strength. Aran *et. al.* [77] used 0.22 μm PES compared to 10 or 70 kDa membranes in our case which is much smaller thus more surface area which may have played a role in bonding or possibly difference in membrane formation.

After some investigation, it was found that surface functionalized layers of APTES at the bonded interface do degrade over time due to hydrolysis of APTES in water. This was confirmed experimentally when the bonded interface was left in water for a few hours. APTES degradation also may be the reason for this bonding method to be employed in gas separation devices with PES membranes and not in aqueous environments [75], [77], [79]. Lee K *et. al.* [80] claims APTES hydrolytic stability is achievable with large thick cross-linked coatings with BTISPA (bis-trimethoxy-silyl-propyl-amine aged for two weeks) since bis-amines cause higher cross-linking within the interface. Although this may prolong the lifetime of the device, it does not stop water from hydrolyzing APTES or BTISPA eventually causing the interface to delaminate.

4.4 Other PDMS to Polymeric Membranes Bonding Methods

Since there were no direct ways ensure a permanent strong bond between PDMS and PES, other bonding techniques between PDMS and polymers in general were considered.

PDMS can be bonded to polymers in several methods via solvent assisted [81], chemical (adhesive intermediates) [82], and plasma treatment [81], [83], [84].

Solvent assisted bonding is the application of pressure to a partially cured substrate or partially dissolved substrate placed with another substrate to cause a blending of the interface material. A strong bond is formed once solidified. However, this requires the polymers to have small molecular weight that is not possible with commercial ultrafiltration membranes. Also, the use of dissolution or thermal reflow can cause blockage of pores in the membrane [85].

Chemical methods of bonding use an intermediate adhesive that bond to both substrates. Chemical bonding materials used with PDMS are silanes such as 3-Aminopropyltriethoxysilane (APTES), 3-aminopropyltrimethoxysilane (APTMS), and 3-glycidoxypropyltrimethoxysilane (GPTMS), 3-Glycidoxypropyltriethoxysilane (GPTES), 3-glycidoxypropylmethyldiethoxysilane (GPMDES), bis-trimethoxy-silyl-propyl-amine (BTMSPA), bis-triethoxy-silyl-propyl-amine (BTESPA), and bis-triethoxy-silyl-ethane (BTESE) in which the silane end bonds to PDMS and one optional group is tailored to specific polymers. All silane intermediate adhesives have issues with hydrolytic stability unless multiple layers of alternating crosslinking silanes are added to resist hydrolysis. This merely extends the lifetime and does not completely prevent bond weakening.

Lastly, plasma treatment is used extensively in microfluidics to bond several substrates. Typically in microfluidics, the bonding process using plasma process employs oxygen or air. If high energy via electric field is applied between two electrodes separated by a dielectric medium such as air, it results in electric discharge causing a cloud of ions and radicals known as a fourth state of matter called plasma. This mixture of ionized gas molecules are ionized and radicalized migrating to one of the electrodes where they can chemically attack the substrate and incorporate surface groups, such as hydroxyl group. When two surfaces are successfully treated with oxygen plasma, the oxygen plasma creates surface dangling hydroxyl groups. The hydroxyl groups can

form a bond between two materials when the substrates are placed in contact together. However, some materials (mostly pure hydrocarbons) are resistant to oxygen plasma treatment as their internal bond strengths are higher and do not form surface functional groups of sufficient density. Oxygen plasma treatment of PES membrane and PDMS did not produce effective bonding with high bond strength.

Although unsuccessful, surface functionalization other than hydroxyl groups, such as fluorine could potentially induce bonding. It is noted in literature that both polyethersulfone and PDMS susceptible to fluorination [86], [87], [88]. Also, SF_6 plasma was demonstrated to bond Parylene-C and PDMS irreversibly by P. Rezai *et. al.* [89] even though Parylene-C does not typically bond with PDMS. Therefore, an initial experiment was designed around the same parameters used by P. Rezai *et. al.* [89] and performed to investigate if the same bonding process of SF_6 plasma in PDMS with Parylene-C applies to PDMS with PES.

4.5 Process Flow

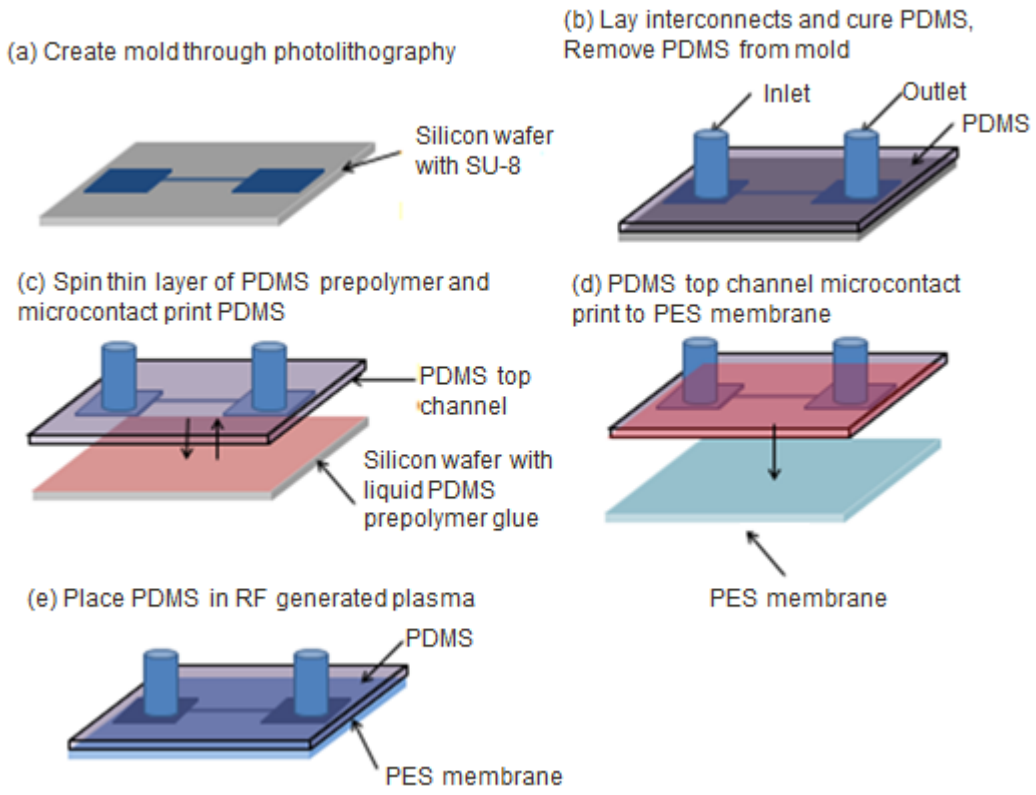

Figure 25: Step-by-step assembly process of the adhesion of PDMS to PES

The process flow for the assembly and bonding process is presented in Figure 25. Starting at Figure 25 a), a mold used to cast the PDMS was made through photolithography techniques using SU-8 2075 as a photoresist. The first experimental molds were a simple channel configuration of 400 µm x 60 µm channels with 3 cm length. The inlets and outlets peroxide cured silicone tubing although variations to the dimensions occur later on. The step-by-step experimental method for photolithography techniques to create a PDMS mold is laid out in Appendix A. The mold for PDMS is shown below in Figure 26.

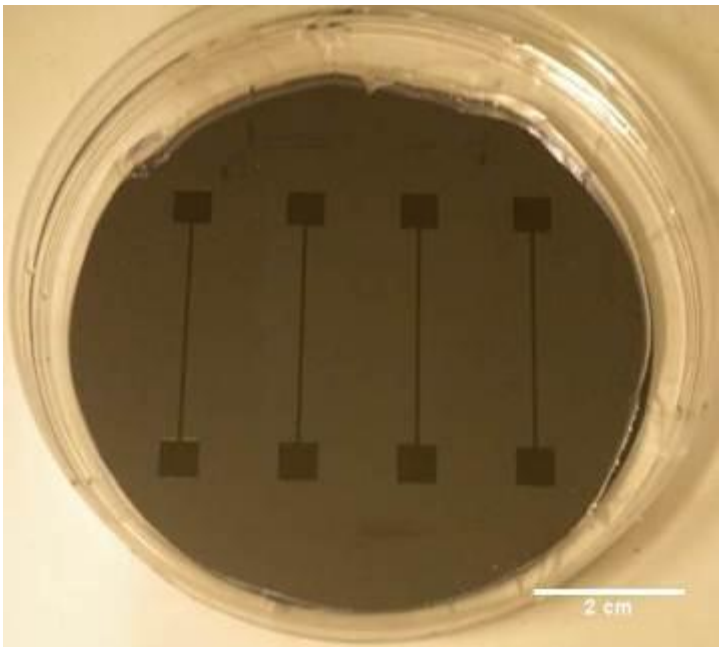

Figure 26: Final mold product from photolithography using SU-8 2075

After the mold was created seen in Figure 26, the PDMS microchannels were fabricated by casting Dow Corning Sylgard 184 PDMS in 10:1 ratio in the master mold with silicone tubing placed on the SU-8 in the mold in before casting as shown in Figure 27 and as step b) in schematic Figure 25. Silicone tubing acts as interconnects to connect to syringe pump for testing. There is a slight adhesion of the silicone tubing interconnects to the SU-8 which usually limits PDMS seeping into the tubing.

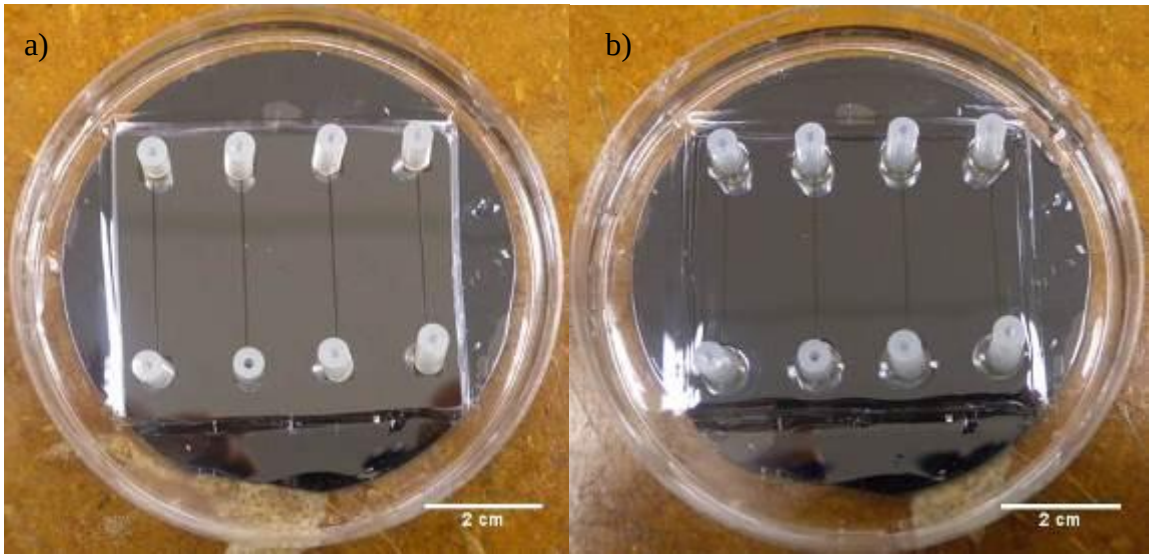

Figure 27: Silicone tubing as interconnects with slight adhesion to SU-8 pads before PDMS (a), after PDMS (b)

After the PDMS cures, the devices were carefully removed by cutting it out using a scalpel. If the interconnects are blocked with PDMS, the cured PDMS is removed by forcibly pushing the plugged PDMS from the silicone tubing using a blunted needle tip or hole punch as shown in Figure 28.

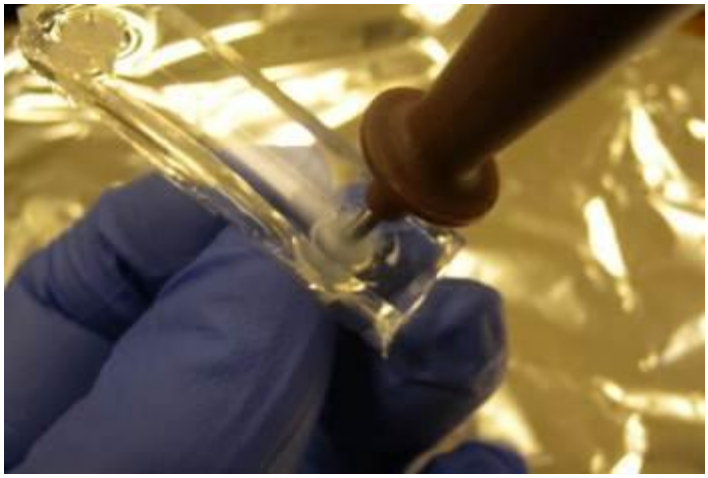

Figure 28: PDMS-plugged interconnect cleared by 1.5mm hole punch

Samples are transferred and handled in a clean room for the subsequent steps to limit contamination. Next, uncured pre-polymer PDMS glue were dispensed on a silicon wafer and

spun at 7000 rpm for 1 min to form a thin layer of PDMS on the silicon wafer seen in schematic Figure 25 c) and Figure 29.

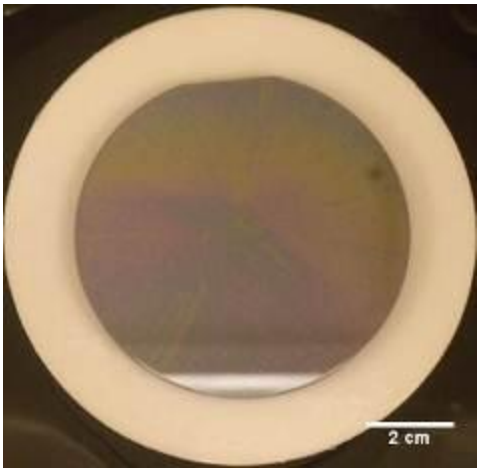

Figure 29: PDMS spun onto silicon wafer at 7000 RPM for 1 min.

This pre-polymer glue serves as a sealant filling the gaps between the uneven PES surface and the PDMS microchannel layer. The PDMS microchannel layer is microcontact printed onto the thin PDMS glue on the silicon wafer to transfer a thin layer of pre-polymer glue onto the contacted parts of the device as shown in Figure 30.

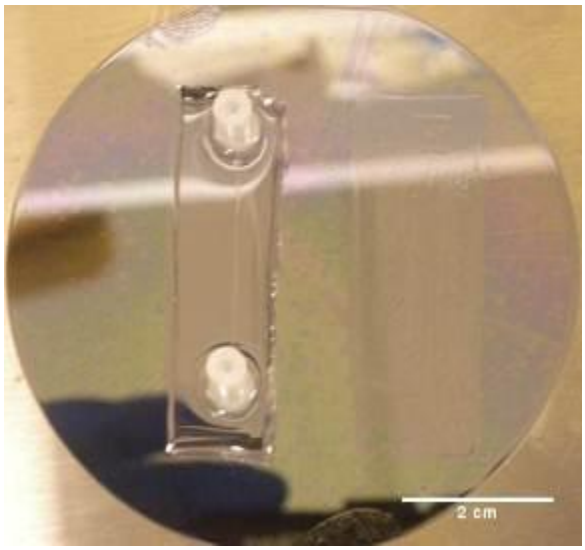

Figure 30: One PDMS channel stamped onto Si wafer and channel imprint when PDMS channel is removed

The microchannel layer is subsequently contacted with the PES membrane shown in schematic Figure 25 d) and in Figure 31. The device is left in contact with membrane for 5 mins before transferring to a hot plate at 70°C to increase the speed of curing.

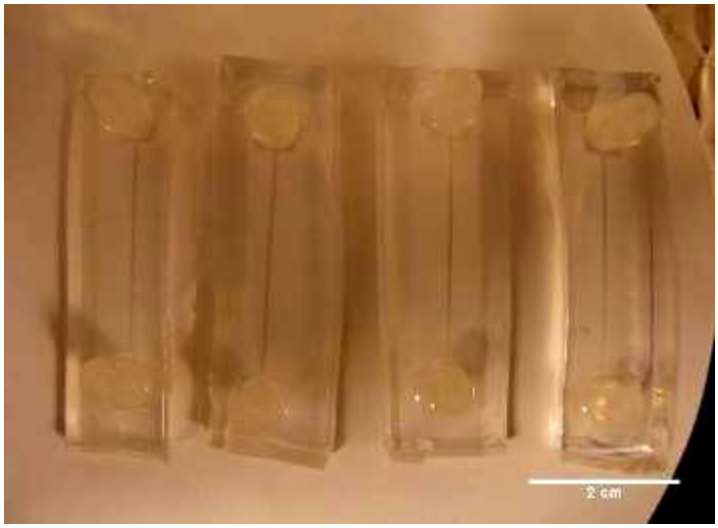

Figure 31: Four PDMS channels stamped onto PES membrane

After the heating, the device is left overnight (12 hrs) and diced before it is ready to be treated with SF_6 plasma in Schematic Figure 25e).

SF_6 plasma was created using D-RIE chamber (Surface Technology System STS-320PC) which generates plasma at 13.56 MHz using radio frequency. The same initial setting used by P. Rezai *et. al.* [89] was implemented in proof-of-concept where flow rates of 30 sccm for SF_6 and 50 sccm for N_2 injected gas into the chamber. The chamber pressure was kept at 50 mTorr and plasma was applied at 300W for ranges of 1 to 3 hours. The final bonded device is shown in Figure 32.

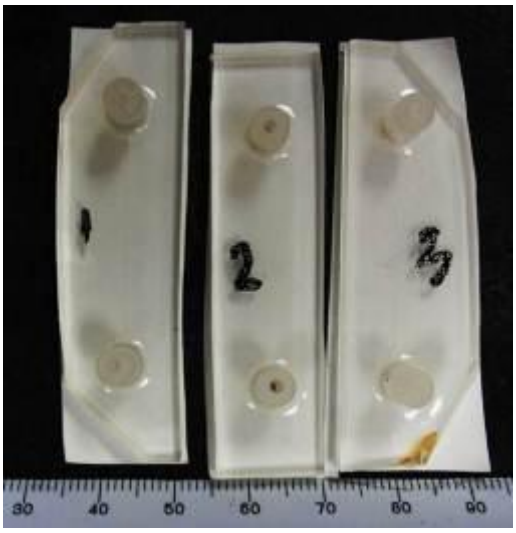

Figure 32: Microchannel test samples after treatment from 3H of SF_6 plasma

Initial qualitative bond strength testing is performed by manually peeling the two bonded surfaces. When peeled, the polyolefin backing detaches from the PES, and the PES layer remains bonded to PDMS indicating a good bond. Even samples that were bonded a year ago demonstrate this effect as shown in Figure 33. This clear indication of good bond strength prompted further investigation.

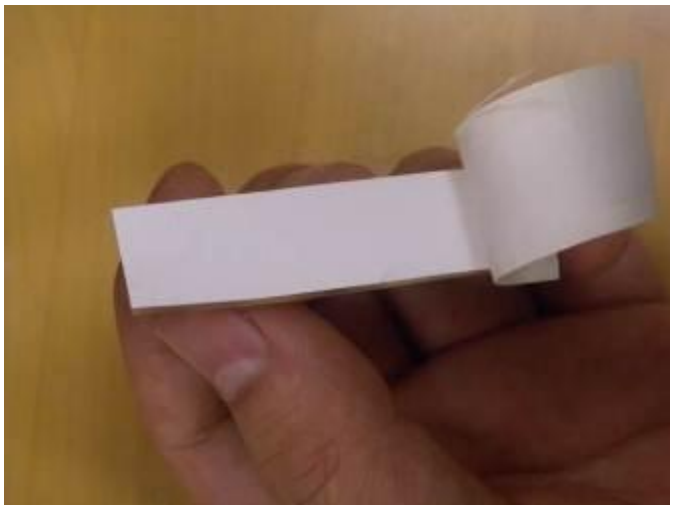

Figure 33: One year old sample treated with SF_6 plasma for three hours with backing peeled

4.6 Bonding Strength Quantification

Quantification of the bonding strength was tested two separated ways; Tensile Pulling and Burst Pressure. Two tests were designed to determine the bonding strength between the PDMS and the PES using two different mechanisms to give different perspective on bonding strength.

4.6.1 Tensile Pull Test Setup

Tensile pull test involves two substrates that are pulled apart using mechanical stepper motors at constant rates. These tests were performed on Instron Tensile Tester. The bonded specimens were cut into a size of 15 mm × 15 mm and glued to steel jigs using two-part Araldite rapid epoxy. The epoxy was cured for 24 h at room temperature. The glued specimens were tested with 1mm/min pull rate and the force was recorded with a computer control interface. At the 1mm/min constant pull rate, the failure point was calculated by the point where detected force peaked and was taken as the ultimate tensile strength. The highest point was used since it is correlated to catastrophic failure.

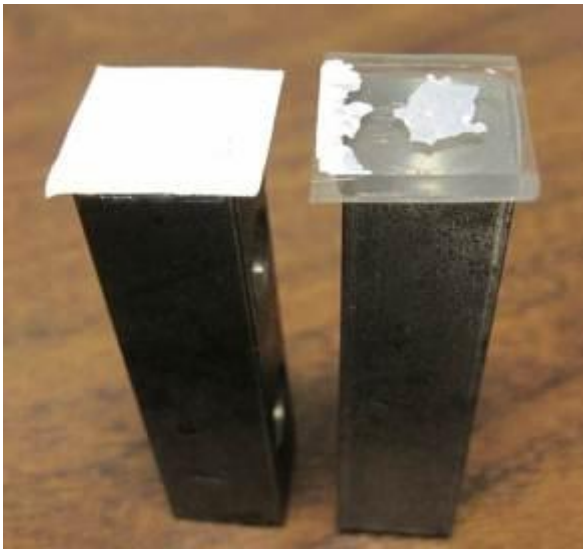

Figure 34: Tensile pull test sample attached to metal chucks after tensile pull test has occurred

4.6.2 Burst Pressure Test Setup

Burst pressure tests measures the maximum pressure a device can withstand before delamination. These tests are more realistic compared to tensile pull test since the quantification gives practical data for conditions similar to when a device is in use. As shown in Figure 35, a syringe pump (KDS Legato 270, KD Scientific Inc., MA, USA) provides constant flow into a T-junction where the branched-end is connected to a pressure sensor (PX273–300DI, Omega Engineering Inc., CT, USA) and the other end is connected to the device. The pressure sensor relays pressure as voltage reading which is connected to a DMM (National Instruments ELVIS DAQ DMM) and recorded on a computer using Labview Signal Express at 2 Hz. The voltage is converted into pressure using a calibration chart. Most connections are made using medical interconnects purchased from QOSINA.

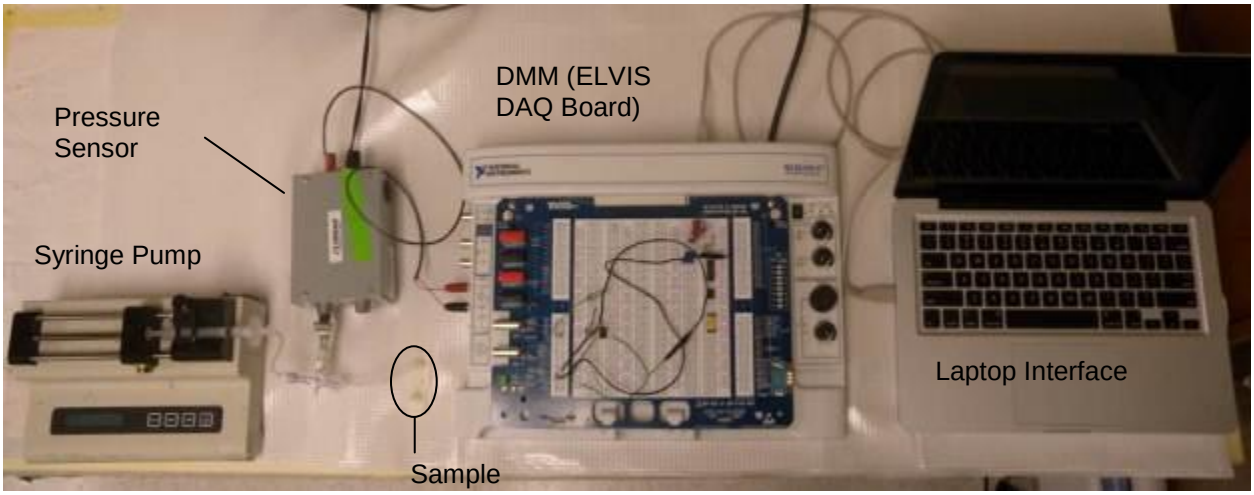

Figure 35: Burst pressure test lab setup

The microchannels were pre-filled with DI water at a flow rate of 50 µl/min via syringe pump with the backing of the membrane open to air. Once filled the outlet was sealed using a cap to allow pressure buildup. The flow rate is then increased up to 120 µl/min until a burst occurs in the device. Devices were measured at different plasma exposure times for comparison.

4.6.3 SEM/EDX

Scanning electron microscopy does not necessarily provide quantitative data on the strength of the bonding, yet the tool is particularly advantageous in visually inspecting the bonding area and channel areas for quasi-quantitative inspection. Additionally, electron dispersive x-ray spectroscopy which is built in within SEM provides information on the mechanism of fluorination and indication of PDMS spread by composition. JEOL 7000F SEM and TESCAN VP SEM were used coupled with Oxford Inca Energy Dispersive Spectrometer for EDX. Samples were prepared by cryogenic freezing with liquid nitrogen and diced using a razor blade. Freezing was required to minimize the effect of dicing on the composition and the

structure of the bonded interface. SEM samples were placed on aluminum stubs, attached using carbon tape and covered with gold using sputtering to reduce charging (image deformation in SEM) since PES, PDMS and Polyolefin are non-conductive materials. Sputtering was done for 1.5 mins at current of 20 mA which converts to a layer of 24Å gold covering the surface.

4.7 Discussion and Results

4.7.1 Bonding Strength Results

The results of the burst pressure test and tensile pull test are shown in Table I and II for different pore sizes of 10 kDa and 70 kDa PES membranes.

Table 5: Comparison of bond strength with 10 kDa polyethersulfone membrane at different durations of exposure to SF_6 and N_2 plasma.

Bonding conditions	Microcontact print bond	Microcontact print plus RIE plasma for 1 h	Microcontact print plus RIE plasma for 2 h	Microcontact print plus RIE plasma for 3 h
Tensile Pull Test Strength [kPa]	19.0	128.6	184.0	192.9
Tensile Pull Test Standard Deviation [kPa]	3.2	10.9	2.8	8.6
Pressure Burst Test Strength [kPa]	20.9	50.9	70.2	86.6
Pressure Burst Test Standard Deviation [kPa]	1.8	5.0	7.3	14.4

Table 6: Comparison of bond strength with 70 kDa polyethersulfone membrane at different durations of exposure to SF_6 and N_2 plasma.

Bonding conditions	Microcontact print bond	Microcontact print plus RIE plasma for 1 h	Microcontact print plus RIE plasma for 2 h	Microcontact print plus RIE plasma for 3 h
Tensile Pull Test Strength [kPa]	19.0	188.6	257.6	269.6
Tensile Pull Test Standard Deviation [kPa]	3.9	4.2	4.1	3.4
Pressure Burst Test Strength [kPa]	27.7	82.6	101.8	146.9
Pressure Burst Test Standard Deviation [kPa]	1.3	11.9	7.8	19.9

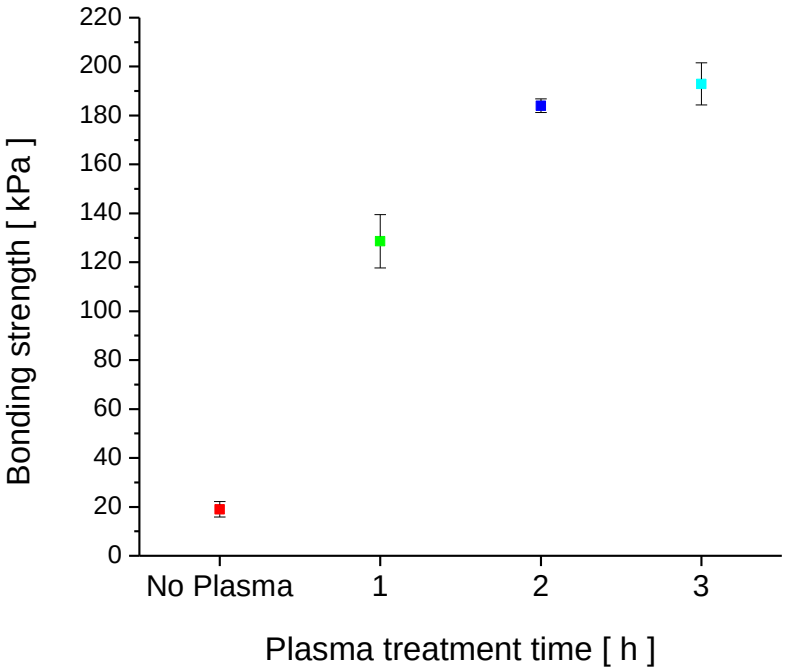

Figure 36: Tensile pull test data from Table I with 10 kDa polyethersulfone membrane at different durations of exposure to SF_6 and N_2 plasma.

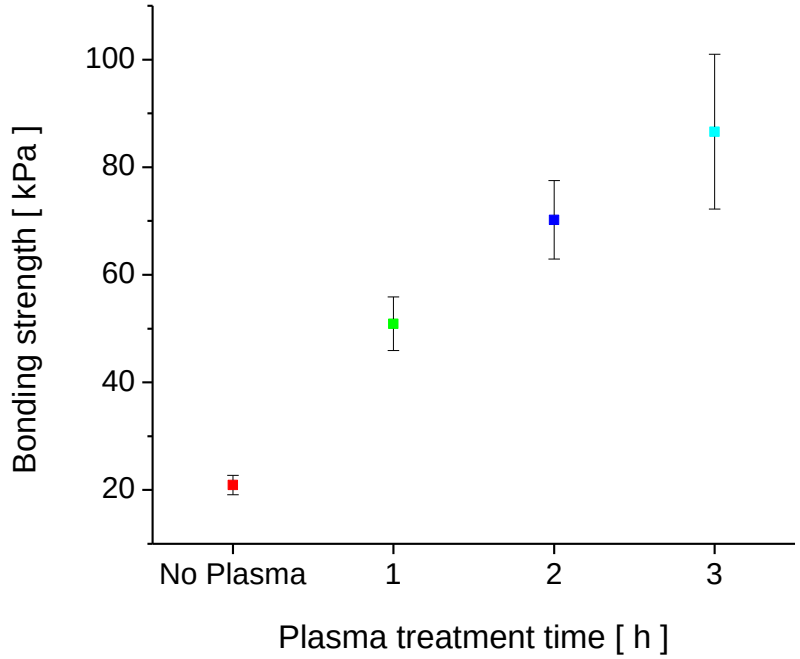

Figure 37: Burst pressure test data from Table I with 10 kDa polyethersulfone membrane at different durations of exposure to SF_6 and N_2 plasma.

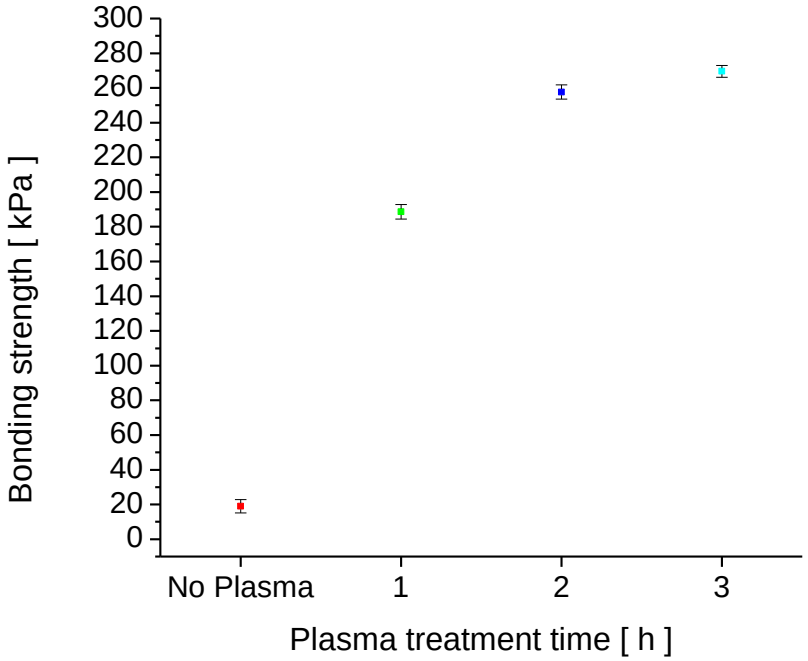

Figure 38: Tensile pull test data from Table II with 70 kDa polyethersulfone membrane at different durations of exposure to SF_6 and N_2 plasma.

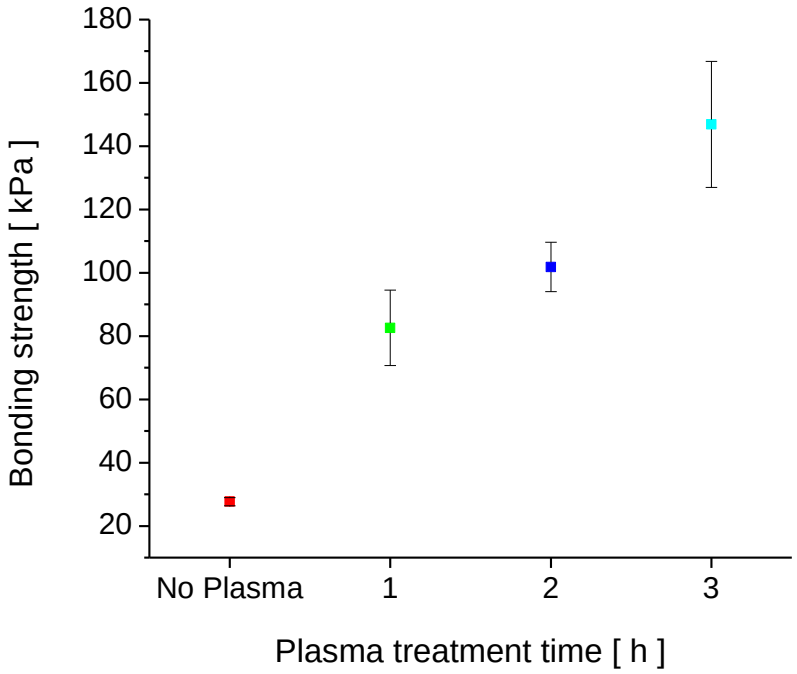

Figure 39: Burst pressure test data from Table II with 70 kDa polyethersulfone membrane at different durations of exposure to SF_6 and N_2 plasma.

From Table I and Table II, a sharp increase in average bond strength is observed between the case when no plasma is applied to when one hour of SF_6 plasma is applied in both the tensile pull test and burst test. The bond strength for the tensile and the burst test was 109.6 kPa and 30 kPa for 10 KDa polyethersulfone membranes and 169.6 kPa and 61.7 kPa for 70 KDa polyethersulfone membranes respectively. For both pore size membranes, bond strength increases with longer exposure times from one hour to three hours. The correlation of bond strength to exposure time could be explained by the greater plasma penetration into the PDMS-polyethersulfone membrane interface with increase of time during the RIE plasma process. In burst pressure and tensile pull test results, the effect of plasma saturates after prolonged exposure as seen by the small increase between two to three hours exposure which is significantly less

than that between one to two hours exposure. Therefore, there is a strong correlation that the more time applied, the stronger bond with diminishing returns over time until all interface sites have been saturated resulting in no more improved bonding. It is expected that four hour plasma experiments will provide little to no improvement of bonding strength. The microcontacted printing interface without any plasma has poor bonding strength and immediately delaminates at 20 kPa.

A clear difference of bond strength between the tensile pull test and the burst is observed throughout all the results. The tensile pull tests reports nearly double the bond strength compared to burst tests and have lower standard deviation. The difference possibly relates to the failure mechanism in each test. In tensile pull tests, the force is applied on the outside from a clamping mechanism causing the force normal to the bond interface and thus measures normal stress force. After the catastrophic failure point, the dense layer of the polyethersulfone membrane separates from the polyolefin base support and remains on the PDMS after the tensile test seen previously in Figure 34 instead of delaminating cleanly from the interface. The residual PES membrane suggests that the bonding strength normal to the bond interface is stronger than the polyolefin backing attachment to the PES membrane surface. Comparatively, the burst test applies force isotropically at the interface via liquid (water) through an inner channel causing a lateral and parallel force directly to the interface. Since the pressurized fluid applies force isotropically, normal and shear forces are applied from the inside at the interface. Furthermore, the burst test failure will usually occur at the weakest bonded areas which results in much lower values and much higher variation.

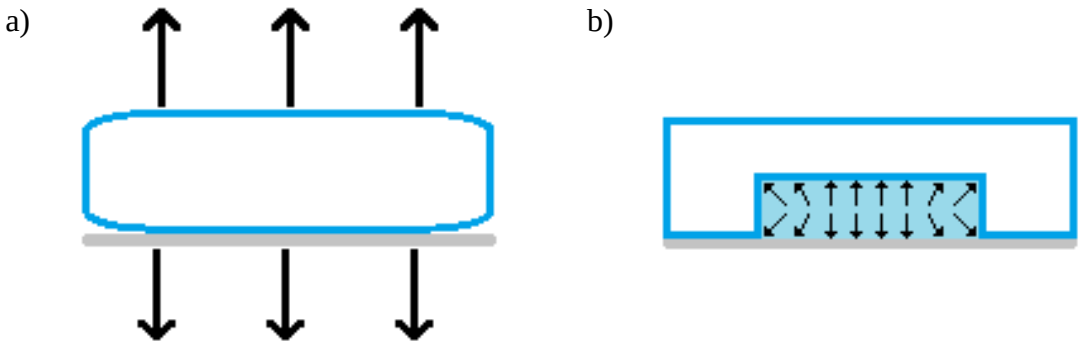

Figure 40: Diagrams illustrating the direction of force in tensile pull test and burst pressure tests. (a) The tensile test failure mechanism is from delamination occurring instantly from the outside inwards only measuring the bonding strength normal to the interface. (b) The burst pressure test uses a liquid medium to apply force causing delamination from the inside outwards. The force is applied to all the inside walls of the channel and attacking the membrane interface isotropically.

There is a noticeable variation in the bonding strength between the two pore sizes. The 10 kDa membrane has significantly lower bonding strength compared to 70 kDa membranes in burst pressure and tensile pull tests. There are two possible factors contributing to the increase of strength; the ease of access of plasma to interface and PDMS diffusion into membrane. The larger pore sizes may increase the ability of plasma to access the interface of the PDMS and polyethersulfone membrane through the fibrous back end which causes better bonding. The second factor is that larger pore size may result in deeper penetration of the PDMS into the pores during microcontact printing. The PDMS would be more deeply rooted causing stronger bonding. Smaller pores would limit the flow of PDMS into the membrane as the PDMS begins to crosslink resulting in less "rooting". Further testing would need to be done to support this hypothesis.

4.7.2 Plasma Bonding Mechanism

Although plasma chemistry is fairly complicated, the proposed mechanism of bonding is explained in P. Rezai *et. al.* [89] and J. Hopkins *et al.* [48] where the highly reactive fluorine

radicals originating from SF_6 plasma causes an intermediate bond to PDMS or polyethersulfone indiscriminately. The unstable radical intermediates attacking the surface most likely causes a methyl and hydride groups to break off to reach lower energy causing a localized free radical on the oxygen or benzene in polyethersulfone [91]. Free radicals at the interface would indiscriminately cause bonding between the two substrates. The nitrogen gas assists the bonding process by acting as a carrier gas for SF_6 and becoming an energized metastable intermediate in plasma.

The manner in which F radicals reach the interface can be spectroscopically analyzed through energy-dispersive X-ray spectroscopy (EDS) as residual fluorination after the bonding process. EDS is an elemental analysis detected by the emission of an X-ray from the de-excitation of ground state electrons from discrete energy levels. Ground state electrons are excited through the transfer of momentum energy by a stream of electrons created by the SEM. The energy of X-ray emission corresponds to the specific energy shells in different elements determining the various elements present. The amount of X-ray emissions counted at various energies compared to the total amount of counted X-ray emissions determines percentage of a certain element in the sample.

D-RIE is generally known to produce unidirectional bombardment with ions considering the intention of D-RIE is for deep etching process. Thus initially, fluorination was thought to be occurring on the PDMS.

The cross-section of the PDMS from top to bottom was sectioned of 4 mm thickness and measured in approximately five equidistance areas in EDS shown by Figure 41. The purpose was to determine if any fluorination would permeate through the PDMS. No residual fluorine was found and only elemental carbon, oxygen, and silicon was found corresponding to the chemical

structure of PDMS seen in Table 7. The EDS readings were measured in areas A – E seen in Figure 41.

Table 7: EDS reading of cross-section of PDMS seen in Figure 41 bonded to PES using SF_6 plasma for 3H

	A (At%)	B (At%)	C (At%)	D (At%)	E (At%)
Carbon	68.0	71.5	71.8	72.7	72.3
Oxygen	5.7	6.2	6.5	6.4	6.3
Silicon	26.4	22.4	21.7	20.9	21.4

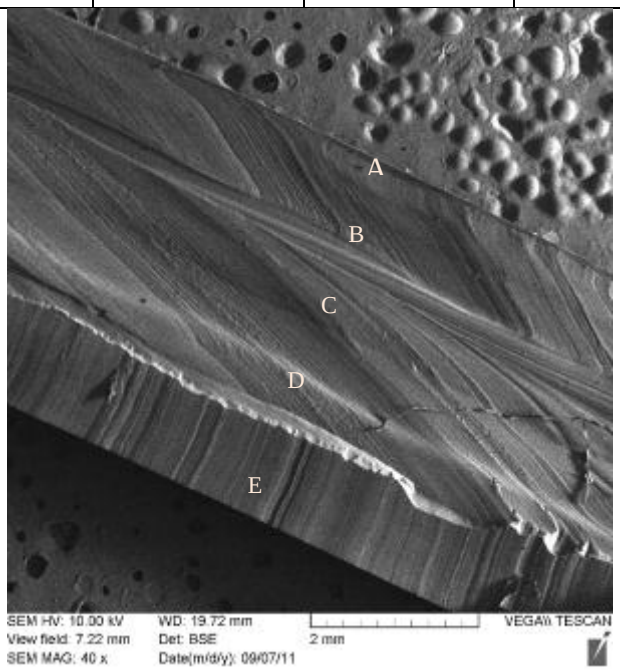

Figure 41: EDS spot readings of cross-section of PDMS block treated to SF_6 for 3H

The sample backend was measured with EDS to observe if plasma was travelling through the back end of the sample. Three randomly selected areas were measured with EDS seen in Table 8 to determine the fluorination occurring on the polyolefin backing from 1 day old samples.

Table 8: EDS results from three randomly selected areas from the polyolefin backing of the PES membrane

	Middle (at%)	Near Center (at%)	Outer (at%)
Carbon	99.18	99.08	98.57
Oxygen	0.17	0.27	0.19
Fluorine	0.64	0.52	1.07
Silicon		0.13	0.16

Some residual detection of fluorine (0.64% - 1%) was seen at the polyolefin backend of the PES which indicates the main entry method of fluorination occurs from behind. Radical species from the plasma must be diffusing into the sides and backend of the membrane. The mean free path at the operating pressures was 1.35 mm assuming no gas flow at ideal gas conditions without Debye shielding effects and kinetic energy from plasma. In reality, the mean free path would be much smaller. Regardless, this is smaller than the dimension of the plasma chamber and hence the radical species in the plasma approach the device in all directions.

4.7.3 Permeation

Although the bonding strength in samples is quite robust, burst pressure test samples did not show any form of permeation of fluid through the membrane. Several reasons were identified as possible causes such as very small pores, air-filled pores, and possibly pore blockage during microcontact printing. Wetting the membrane in water-ethanol mixture and then perfusion did not induce permeation indicating that wetting is not a problem. The interface was separated and analyzed under SEM to possibly determine blocking via PDMS seen in Figure 42

Energy-dispersive X-ray spectroscopy was performed on the inside of the channel from a bird-eye view after the PDMS was removed and showed 4-5% of atomic weight silicon within

the channel. From the composition of the substrates, it was deduced that the presence of silicon must originate from PDMS since PES has no traces of silicon. Furthermore, the EDS of polyolefin backing in

Table 8 found trace amounts (< 0.2%) of silicon. This was surprising since no visual indication of PDMS is seen on the membrane as shown in Figure 42 a) where the topography in the channel area is similar to unblocked PES membrane. There are no overlapping elemental X-ray count peaks on silicon indicating PDMS is on the surface of the channel in a non-observable manner.

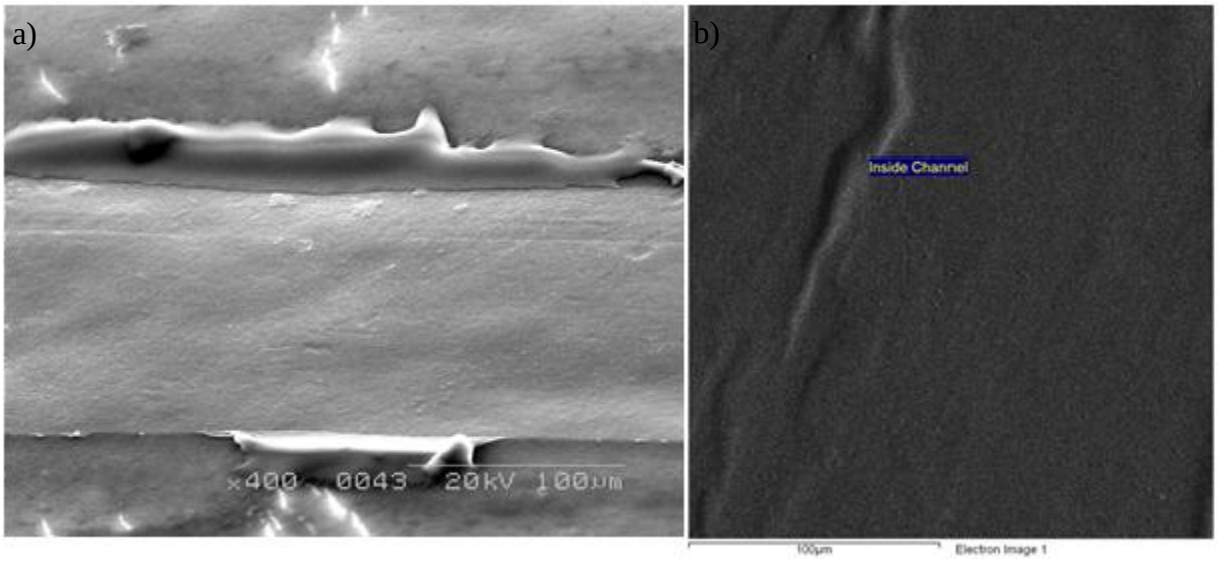

Figure 42: (a) SEM image of PES membrane at 60 angle tilt in channel area after PDMS top removed. Sample was measured at angle to clearly observe the surface topography. (b) First EDS image reading location inside channel indicating 4.86 At% of elemental Si K

The presence of PDMS in the channel region can be attributed to two possible scenarios. First, PDMS pre-polymer could have spread laterally from the microcontact printed regions forming a thin membrane invisible under SEM and blocking the pores of the membrane. Second, PDMS could have been etched and deposited on the surface as a thin film due to plasma inside the channel. The second scenario seems less probable since there is no direct access of the

interior of the microchannels to the conditions in the plasma except through the polyolefin backing. Therefore, it was assumed that the PDMS pre-polymer spreading during microcontact printing could be the reason and various modifications were developed to mitigate it.

4.7.4 Mitigation of PDMS Spreading

A number of process modifications were investigated to mitigate the spreading of the PDMS pre-cursor glue into the micro channel. The first was to decrease the amount of PDMS used in contact with the membrane limiting the contacted areas with a thin layer of PDMS. Therefore, hexane at 20% and 33% by weight was added to the uncured PDMS glue before spinning to allow thinner films of PDMS for microcontact printing. The thickness of PDMS post-spinning on the Si wafer is estimated to be 300-400 nm for 20% and 33% weight using Thangawng *et. al.* [92] chart for hexane dilution relative to ~1-3 μm without hexane.

The solution was spun at 6000 rpm for 1 min on Si wafer and rested for 15 min to allow hexane to evaporate and from a thin layer of PDMS. The hexane modification enhanced the PDMS spreading problem by increasing the rate of PDMS spreading and weakening bonding strength. The weaker bonding may have been due to fact that the thickness of the adhesive layer (PDMS pre-polymer) was smaller than the roughness of the 70 kDa PES membranes. The roughness of the membrane was determined using white light interferometry (ZYGO). Five scans were performed giving a 3D plot and a line profile was taken. The average roughness is determined to be 1.38 μm which is much greater compared to the 300- 400 nm layer of PDMS glue.

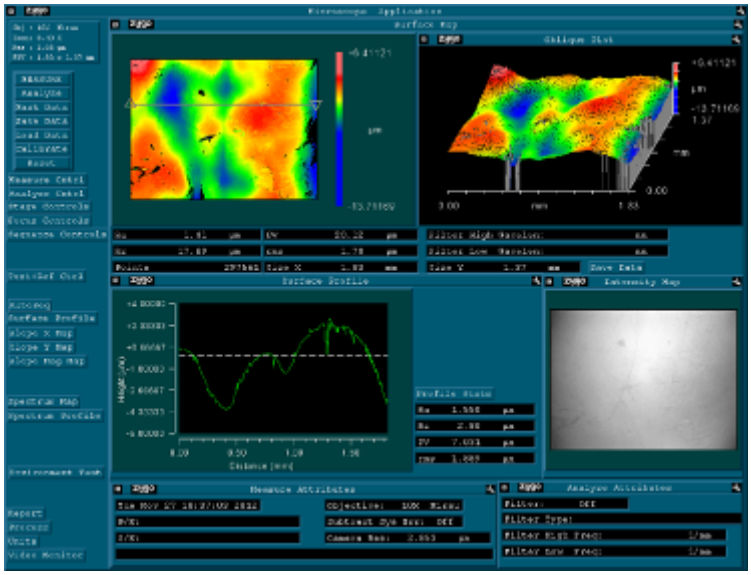

Figure 43: Screenshot of ZYGO user interface analyzing 70KDa membrane topography. Top right shows the 3D representation of membrane surface. Top left indicated line profile reading shown bottom left. Areas that are black are places where no data was collected possibly to corner effects. Average roughness is calculated using the profile line.

Another modification was to instantaneously polymerize the PDMS pre-polymer adhesive layer once it comes in contact with the ultrafiltration membrane after microcontact printing by placing the microcontact printed device on a hot plate at elevated temperature. Samples were microcontacted onto membranes that were heated to 90°C in attempts to cure the PDMS before it spread to non-contacted regions. The PDMS did cure quicker as seen visually in Figure 44. However, large cavities were also formed as the PDMS could not spread to the entire contacted region and form a conformal seal to the membrane surface. These cavities would significantly reduce the burst pressure for failure and could also increase the variation in bond strength. Different combinations of heating and coupling with plasma oxygen were attempted but none of the results gave permeation regardless or burst before permeation occurred.

Figure 44: μCP sample after heated membrane process of 90°C

Another modification was to expose oxygen plasma through a mask such that the microchannel region is protected. Oxygen plasma treatment increases wetting of PDMS and selective exposure in the contact areas will enable a quicker spreading there. In this scenario, by coupling oxygen plasma with heating, PDMS will spread in oxygen plasma exposed regions around the microchannel quickly covering all exposed areas before the heating process causes polymerization, halting the spreading process. This ensures no air bubbles are found in proximity of the microchannel. The area near the microchannel not exposed to oxygen plasma will spread at a normal rate.

The area near the channel area was blocked from plasma oxygen exposure using scotch tape. Several different combinations were performed using 7000 rpm spin speed, wet contact and 1.2 mm wide channels.

Table 9: Coupling plasma oxygen with various tape coverings for mitigation of PDMS spreading

Plasma Oxygen Side	Tape Side	Heated?	Result
Membrane Only	Membrane	No	Tape Stuck on Membrane
PDMS, Membrane	Membrane	No	Tape Stuck on Membrane
PDMS, Membrane	PDMS	No	PDMS Spread To Fast
PDMS Only	PDMS	No	PDMS Spread Eventually to Channel
PDMS Only	PDMS	Yes. 80C	Appeared to be no spreading. Determine by EDS

Devices that were heated after treatment with plasma oxygen applied to the PDMS side and with tape covering roughly ~1 mm outwards of the channel showed the most uniform spreading of PDMS with no visually indication spreading of PDMS into the channel. The top PDMS device was removed and EDS analysis was performed on channel area after DRIE and EDS was performed near the center of the channel.

No trace of atomic Si was found which indicated that PDMS did not spread to the center of the microchannels. These devices showed permeation with ethanol during burst tests but not with water. Channel widths were modified to produce permeating channel even with some amount of spreading. Two channels with widths of 3.3 mm and 4.6 mm were made, and shown in Figure 45

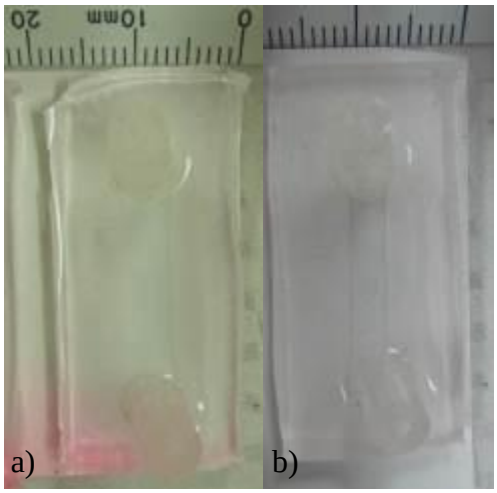

Figure 45: (a) 4 mm and (b) 3 mm wide channel with PES 70 kDa membrane with Rhodamine B/PDMS intermediate glue as indicator

These large channels showed good bond strength as well as permeation. There was visual indication of the PDMS pre-polymer ingress (~100 μm) into the channel region, either due to spreading or due to slippage during the microcontact printing. However, as seen in Figure 46, the central region of the microchannel had the pores open and there were clear signs of permeation of water and ethanol through the membrane.

Figure 46: Permeation of water/ethanol in 3.3 mm large channel device during burst pressure test

EDS was performed on the permeating channel to determine the presence of PDMS within the channel from either spreading or redesposition. Five-point spectrum was taken at different depths of the cross-section seen in Figure 47. There is a slight deformation and compression of the membrane down due to cutting the membrane with a razor in the Figure 47

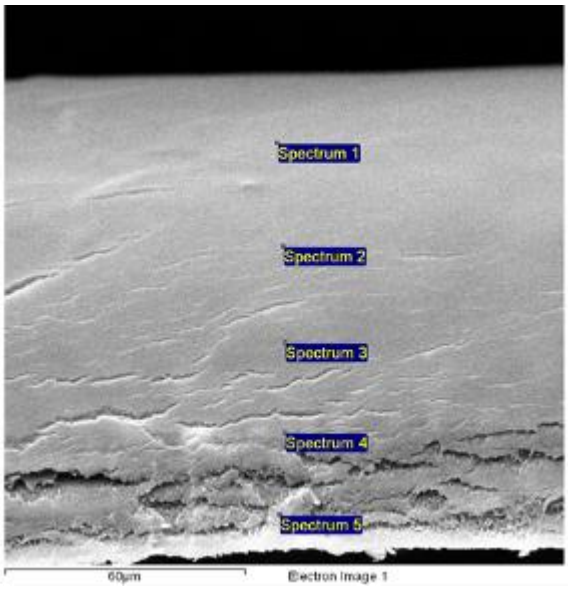

Figure 47: Five spectrum points taken from a cross section cut of the channel device 3.3 mm channel treated with SF_6 and N_2 plasma

Table 10: EDS spectrum reading of the five points taken in Figure 47

Spectrum Number	Carbon (at%)	Oxygen (at%)	Silicon (at%)	Sulfur (at%)	Chlorine (at%)
Spectrum 1	84.47	5.22	1.58	8.74	
Spectrum 2	82.52	4.74	1.52	11.21	
Spectrum 3	82.25	4.14	1.17	12.12	0.31
Spectrum 4	81.64	3.88	1.29	13.19	
Spectrum 5	83.74	4.06	0.4	11.54	0.25

The results show that there were small traces of silicon indicated a presence of PDMS but in extremely low amounts. This may be due to the redeposition of Si instead of PDMS of spreading with in the membrane which cannot be avoided. Therefore, it was concluded that the

PDMS did not spread into the microchannels. There are traces of chlorine since this sample was performed after a burst test was performed.

4.8 Microfiltration Pore Size Device

Although the previous experiments were all performed using ultrafiltration membranes, higher throughput for water filtration can be obtained using microfiltration membranes. In a bacteria filtration case, microfiltration membranes would be the appropriate choice. The hydraulic resistance is much lower in microfiltration resulting in greater amount of permeate flux for transmembrane pressure (TMP) seen previously in Equation (2) in Section 3.3.1 . This reduction is hydraulic resistance is important in order not to cause delamination of the membrane during operation. Furthermore, the microfiltration membranes do not have a polyolefin backing making them simpler and allow the possibility of using the same bonding method to bond microchannels to the other side of the membrane. Millipore Express PLUS Polyethersulfone Membrane 0.22 μm disks were used with the original channel configuration of 400 μm x 60 μm channels in 3 cm length. During microcontact printing, an immediate discoloration of the membrane was observed due to the PDMS seeping into the membrane and samples were heated immediately after microcontact at 90°C. Samples were placed under 3H and 2H SF_6 plasma under the same conditions.

Burst pressure test was performed on samples at 50 μl/min with membrane back-end open to atmosphere. For 2H and 3H samples, samples treated with ethanol/water permeated at 50 μl/min with no pressure build up. Flow rate was continually doubled when permeation was stabilized and eventually increased to 3.2 ml/min before bursting.

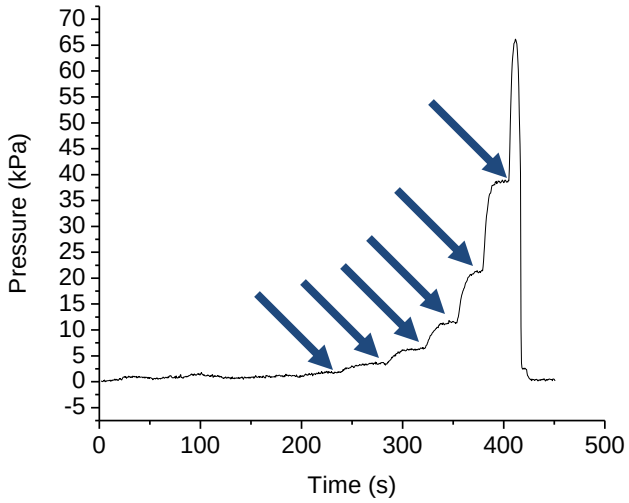

Figure 48: Two hour burst pressure test profile. Arrows indicate where flow rate was doubled

Burst pressure results of three samples were 56 kPa ± 9 kPa for two hour exposure to plasma and 44 kPa ± 9 kPa for three hour exposure with all devices permeating before delamination through pressure build up. This is particular interesting considering that the three hours sample had lower burst pressures indicating a weak bond and needs further investigation. White light interferometry was performed using ZYGO 3D Optical Surface Profiler to determine the roughness of the membrane. Five surface reading at random shows a surface roughness is 0.35 ± 0.05 μm which shows the 0.2 μm PES membrane roughness is lower than the 70 kDa roughness of 1.38 ± 0.096 μm resulting in possibly better microcontact printing. Another explanation is the mechanism of "rooting" which is different for ultrafiltration and microfiltration membranes. Ultrafiltration membranes have decreasing pore size from the backend of the membrane to the front seen in Figure 49 a). Microfiltration has straight pores and do not have a tapering pores comparatively seen in Figure 49 b). These differences are due to the manufacturing method of both membranes. The PDMS on a ultrafiltration membranes will be anchored in the pores due to the pore configuration while PDMS in the microfiltration

membrane will have no obstacles when removed. In addition, there is a higher amount of surface area contact between the ultrafiltration membrane due the number of pores and pore configuration which results in much more interface for the bond to be reinforced.

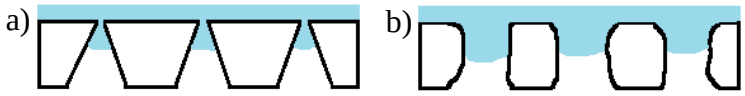

Figure 49: (a) Ultrafiltration membrane pore shape and (b) microfiltration membrane pore shape

After removing the membrane from the PDMS, SEM/EDS of a top view of the membrane shown in Figure 50 shows a clear indication of where the PDMS stopped spreading.

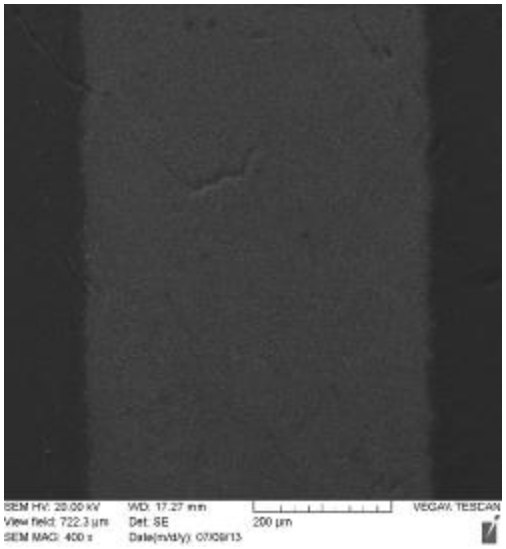

Figure 50: Top view of 0.2 µm PES membrane peeled from a 2H burst sample

The large pores most likely slowed down the PDMS spreading laterally and facilitated spreading downwards as well resulting in no blocking. EDS was performed on the left edge at four spots indicated in Figure 51.

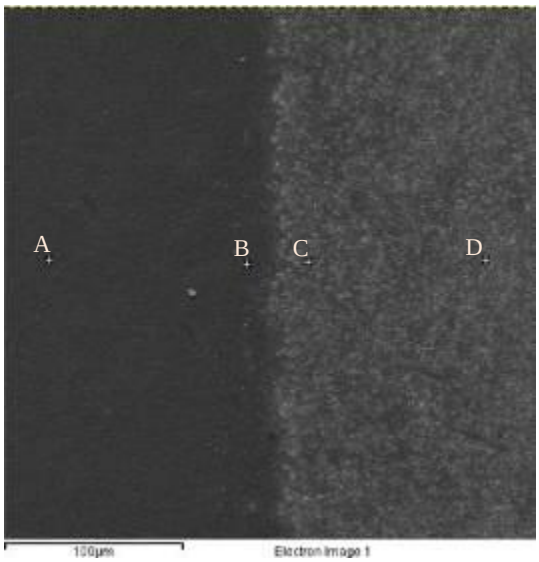

Figure 51: Left edge of microchannel area on 0.2 µm PES Membrane

Table 11: EDS elemental readings of spot spectrums selected in Figure 51

Spectrum	Carbon (at%)	Oxygen (at%)	Fluorine (at%)	Silicon (at%)	Sulfur (at%)	Chlorine (at%)	Nickel (at%)
A	64.59	3.09	0.00	24.32	7.77	0.23	0.00
B	63.22	3.47	0.00	25.41	7.90	0.00	0.53
C	75.83	2.84	0.00	1.90	19.00	0.43	0.00
D	73.43	3.01	1.56	2.43	19.15	0.42	0.40

EDS analysis also showed a drop in Si content inside the channel area indicating that the PDMS did not spread.

4.9 Summary of Experimental Bonding of SF_6 Plasma

The integration of polysulfone membranes within microfluidic devices made of PDMS using SF_6 plasma was successfully demonstrated. The two types of tests, burst pressure and tensile pull, show the effectiveness of SF_6 plasma and indicated bond strengths of 192.9 ± 8.6 (tensile) and 86.6 ± 14.4 kPa (burst) for 10 kDa membrane and 269.6 ± 3.4 (tensile) and 146.9 ±19.9 kPa (burst) for 70kDa treated for 3 hours compared to ~20 kPa bond strength without any plasma treatment. Polyethersulfone membranes with 0.2 µm pores bond strength was 56 ± 9 kPa

treated for 3 hours and permeated 3.2 ml/min before bursting which will effectively filter 1-2 ml of pre-concentration sample under a minute. The steady increase of bonding strength with SF_6 plasma treatment was observed. This is the first report of using plasma processes to bond ultrafiltration membranes with PDMS microchannels.

However, the absence of permeation during a burst pressure test indicated that the pores were sealed. Process modifications were made to ensure that the seepage of PDMS pre-polymer was prevented and a recipe was identified that produced good bond strength and permeation.

Chapter 5 Conclusions

5.1 First Stage Pre-concentration Hollow Fiber Conclusions

As a reminder, the motivation of this thesis was the development of a portable device for affordable, on-site, quick detection of pathological bacteria in drinking water sources using molecular biological methods. The thesis focused on miniaturization of the sample preparation for such a device; specifically it dealt with the development of a filtration unit that would concentrate the content of a large volume of sample into a small eluted volume suitable for the detector. Among the various methods available, only membrane filtration currently has 100% proven retention and high throughput. Hollow fibers were used to fabricate a device with low elution volume and high throughput. The device can be operated using a manual syringe as the pressure source and is simple and portable.

It was found that the recovery of 250 ml samples seeded with 3.0×10^4 *E.coli* bacteria and 2.2×10^3 *E.coli* bacteria resulted in 100% recovery. A lower count of 240 *E.coli* bacteria resulted in 50% recovery, but no detectable CFU were found in the filtrate suggesting bacterial attachment on the membrane.

Filtration times were 10-20 min for 250 ml which is very quick for a single fiber. A one liter sample can be filtered in 40 mins with a 15 cm fiber.

The amount of dead volume (1-2 ml) from the hollow fiber device still is too large to directly send to a biosensor and therefore another filtration step in a microfluidic device integrated with the biosensor is needed where the sample can be further concentrated.

5.2 Second Stage Microfluidic Device Filtration Conclusions

Since the second filtration stage is to be small and has to be integrated with the microfluidic device, bonding methods for integrating flat sheet membranes with PDMS microchannels were devised. Polyethersulfone membrane with 70 kDa and 10 kDa pore size was chosen as the membrane material as they have high porosity, is less expensive, and commercially available. It is known for reduced biofouling which is an issue seen in the hollow fiber device.

The bonding method used was plasma based and relied on surface functionalization of the PDMS and the PES interface using highly reactive fluorine radicals created in plasma from dissociation of SF_6. This method is generic and potentially can be applied to bond a wide variety of commercial membranes with microfluidic devices.

Characterization of the bond strength using tensile pull test and a burst pressure test were performed. Enhanced bonding strength of 192.9 ± 8.6 (tensile) and 86.6 ± 14.4 kPa (burst) for 10 kDa membrane and 269.6 ± 3.4 (tensile) and 146.9 ±19.9 kPa (burst) for 70kDa were achieved at three hours of plasma treatment. A general increase of bonding strength with various amounts of plasma treatment allows tailoring of bonding strength for different applications with a limit of supposed saturation of bonding sites.

5.3 Future Work

The main contribution in this thesis is the characterization of a simple hollow fiber based concentration device for collecting and eluting bacteria from water samples. Another contribution is the bonding of the flat porous membrane with PDMS leading the way to integrate commercial ultra and microfiltration membranes with microchannels. Both these developments

will potentially lead to development of pre-concentration as an alternate method to enrichment in rapid diagnosis of pathogens in water and food samples.

Further improvements are needed in increasing the recovery of the hollow fiber filtration device at much lower concentrations. The exact cause for 50% recovery at 240 *E.coli* bacteria should be investigated. The most likely candidate is biofouling from impact wedging in the pores, but it is possible the bacteria may be lost in the surfaces of the containers used since the amount of bacteria is so low. It is even possible that in the time frame the experiment was performed, the bacteria could have simply died from starvation. A method to confirm the results is with more sensitive detection methods such as fluorescent tagging in a flow cytometer especially on lower order seeding to achieve possibly more accurate results. Other possible method is using GFP-expressing bacteria for a low concentration experiment and observes the fiber under a fluorescent microscope to determine biofouling on the membrane surface.

The second most important improvement to this work is using much larger sample sizes. Sample volumes of 250 ml were used due to limitation on the size of containers used in the autoclave but typical water samples can be from 100 ml to several liters. Larger samples can be characterized to investigate the recovery in much lower concentration.

Lastly, a single 15cm length fiber was used in the design of the hollow fiber device since it was sufficient to perform one liter filtration within 40 mins. Multiple fibers bundled could be configured to filter 10 -20 L possibly for even more possible sample.

The plasma conditions and the recipe for bonding have not been optimized yet. Fluorine plasma experiment kept optimal gas flow condition, chamber pressure, power and time set by Rezai P *et. al.* [89] yet these experiments are optimized for Paralyne C to PDMS. Certain recommendation can be made. First, the increasing the power might cause more aggressive

plasma and increase bonding strength with less time. Secondly, chamber pressure could be increased in order to shorten free mean path of fluorine radicals and further isotropic exposure. Thirdly, the gas flow rates thus the ratio of SF_6 to N_2 could be changed although it is not understood what would be the recommended action in improving bonding strength. Lastly, reversing the orientation of the sample in the plasma where the polyolefin faces upwards will significantly decrease the exposure times but will likely greatly increases the amount of variability. Short bursts of plasma would need to be applied instead of continuous exposure.

In summary, strong ground work for sample preparation using a two-stage filtration and separation device has been done. Further work along these lines can potentially allow pre-concentration of large samples to replace enrichment as the method of choice to analyze water samples.

REFERENCES

[1] A. E. Murray, D. Lies, G. Li, K. Nealson, J. Zhou, and J. M. Tiedje, "DNA/DNA hybridization to microarrays reveals gene-specific differences between closely related microbial genomes," *Proceedings of the National Academy of Sciences of the United States of America*, vol. 98, no. 17, pp. 9853–8, Aug. 2001.

[2] R. Drmanac, S. Drmanac, Z. Strezoska, T. Paunesku, I. Labat, M. Zeremski, J. Snoddy, W. Funkhouser, B. Koop, L. Hood, and al. et, "DNA sequence determination by hybridization: a strategy for efficient large-scale sequencing," *Science*, vol. 260, no. 5114, pp. 1649–1652, Jun. 1993.

[3] Z. Qingdi and D. Trau, "Simultaneous Detetion of Protein and DNA in a Microfluidic Device Using Spatial Addressable Microbeads on a Gel Pad Array," in *14th International Conference on Miniaturized Systems for Chermistry and Life Sciences*, 2010, pp. 455–457.

[4] T. G. Drummond, M. G. Hill, and J. K. Barton, "Electrochemical DNA sensors," *Nature biotechnology*, vol. 21, no. 10, pp. 1192–9, Oct. 2003.

[5] J. Wang, M. Aki, D. Onoshima, K. Arinaga, N. Kaji, M. Tokeshi, S. Fujita, N. Yokoyama, and Y. Baba, "Microfluidic sensor for the detection of DNA or protein by hybridization-based fluorescence enhancement or immunoassay-based fluorescence quenching," in *14th International Conference on Miniaturized Systems for Chermistry and Life Sciences*, 2010, pp. 1514–1516.

[6] T. Sakata, M. Kamahori, and Y. Miyahara, "DNA Analysis Chip Based on Field-Effect Transistors," *Japanese Journal of Applied Physics*, vol. 44, no. 4B, pp. 2854–2859, Apr. 2005.

[7] A. Sassolas, "DNA Biosensors and Microarrays," *Chemical Reviews*, vol. 108, no. 1, pp. 109 – 139, 2008.

[8] P. O. Brown and D. Botstein, "Exploring the new world of the genome with DNA microarrays," *Nature Genetics*, vol. 21, pp. 33–37, 1999.

[9] M. Waleed Shinwari and M. Jamal Deen, "Optimization of DNA detection using FETs," in *2008 1st Microsystems and Nanoelectronics Research Conference*, 2008, pp. 185–188.

[10] U. Dharmasiri, M. A. Witek, A. Adams, J. K. Osiri, M. L. Hupert, T. S. Bianchi, D. L. Roelke, and S. A. Soper, "Enrichment and detection of Escherichia coli O157:H7 from

water samples using an antibody modified microfluidic chip," *Analytical chemistry*, vol. 82, no. 7, pp. 2844–9, Apr. 2010.

[11] J. B. Reece, L. A. Urry, M. L. Cain, S. A. Wasserman, P. V. Minorsky, and R. B. Jackson, *Campbell Biology (9th Edition)*. Benjamin Cummings, 2010.

[12] J. Mairhofer, K. Roppert, and P. Ertl, "Microfluidic systems for pathogen sensing: a review," *Sensors*, vol. 9, no. 6, pp. 4804–23, Jan. 2009.

[13] H. Andersson and A. van den Berg, "Microfluidic devices for cellomics: a review," *Sensors and Actuators B: Chemical*, vol. 92, no. 3, pp. 315–325, Jul. 2003.

[14] T. Fujii, "PDMS-based microfluidic devices for biomedical applications," *Microelectronic Engineering*, vol. 61–62, pp. 907–914, Jul. 2002.

[15] M. Toner and D. Irimia, "Blood-on-a-chip," *Annual review of biomedical engineering*, vol. 7, pp. 77–103, Jan. 2005.

[16] D. J. Beebe, G. A. Mensing, and G. M. Walker, "Physics and applications of microfluidics in biology," *Annual review of biomedical engineering*, vol. 4, pp. 261–86, Jan. 2002.

[17] J. Kim, M. Johnson, P. Hill, and B. K. Gale, "Microfluidic sample preparation: cell lysis and nucleic acid purification," *Integrative biology*, vol. 1, no. 10, pp. 574–86, Oct. 2009.

[18] R. Mariella, "Sample preparation: the weak link in microfluidics-based biodetection," *Biomedical microdevices*, vol. 10, no. 6, pp. 777–84, Dec. 2008.

[19] J. Gao, "Integration of single cell injection, cell lysis, separation and detection of intracellular constituents on a microfluidic chip," *Lab on a Chip*, vol. 4, no. 1, pp. 47 – 52, 2004.

[20] E. A. Schilling, A. E. Kamholz, and P. Yager, "Cell Lysis and Protein Extraction in a Microfluidic Device with Detection by a Fluorogenic Enzyme Assay," *Analytical Chemistry*, vol. 74, no. 8, pp. 1798–1804, Apr. 2002.

[21] C. Zhang, J. Xu, W. Ma, and W. Zheng, "PCR microfluidic devices for DNA amplification," *Biotechnology advances*, vol. 24, no. 3, pp. 243–84, Jan. 2006.

[22] R. H. Liu, J. Yang, R. Lenigk, J. Bonanno, and P. Grodzinski, "Self-contained, fully integrated biochip for sample preparation, polymerase chain reaction amplification, and DNA microarray detection," *Analytical chemistry*, vol. 76, no. 7, pp. 1824–31, Apr. 2004.

[23] M. A. Levin, J. R. Fischer, and V. J. Cabelli, "Quantitative Large-Volume Sampling Technique," *Applied and Environmental Microbiology*, vol. 28, no. 3, pp. 515–517, Sep. 1974.

[24] S. M. Goyal and C. P. Gerba, "Simple method for concentration of bacteria from large volumes of tap water," *Applied and Environmental Microbiology*, vol. 40, no. 5, pp. 912–916, Nov. 1980.

[25] S. Farrah and C. Gerba, "Concentration of viruses from large volumes of tap water using pleated membrane filters," *Applied and Environmental Microbiology*, vol. 31, no. 2, pp. 221–226, 1976.

[26] J. Yang, Y. Liu, C. Rauch, and R. Stevens, "High sensitivity PCR assay in plastic micro reactors," *Lab on a Chip*, vol. 2, no. 4, pp. 179–187, 2002.

[27] J. Min, J.-H. Kim, Y. Lee, K. Namkoong, H.-C. Im, H.-N. Kim, H.-Y. Kim, N. Huh, and Y.-R. Kim, "Functional integration of DNA purification and concentration into a real time micro-PCR chip.," *Lab on a chip*, vol. 11, no. 2, pp. 259–65, Jan. 2011.

[28] R. Ghosh, *Principles of bioseparations engineering*. World Scientific, 2006.

[29] Z.-L. Xu and F. Alsalhy Qusay, "Polyethersulfone (PES) hollow fiber ultrafiltration membranes prepared by PES/non-solvent/NMP solution," *Journal of Membrane Science*, vol. 233, no. 1, pp. 101–111, Apr. 2004.

[30] Z. Xu, Q. Dai, Z. Liu, R. Kou, and Y. Xu, "Microporous polypropylene hollow fiber membranes: Part II. Pervaporation separation of water/ethanol mixtures by the poly (acrylic acid) grafted membranes," *Journal of membrane science*, vol. 214, pp. 71–81, 2003.

[31] S. M. Goyal and C. P. Gerba, "Simple method for concentration of bacteria from large volumes of tap water," *Applied and environmental microbiology*, vol. 40, no. 5, pp. 912–6, Nov. 1980.

[32] Y. Wang, F. Hammes, N. Boon, and T. Egli, "Quantification of the Filterability of Freshwater Bacteria through 0.45, 0.22, and 0.1 um Pore Size Filters and Shape-Dependent Enrichment of Filterable Bacterial Communities," *Enviromental Science and Technology*, vol. 41, no. 20, pp. 7080–7086, 2007.

[33] ASTM International, "Standard Practice for Determining Microbial Colony Counts from Waters Analyzed by Plating Method," *D5465-93*, vol. 93. pp. 1–4, 2012.

[34] J. S. Baker and L. Y. Dudley, "Biofouling in membrane systems - A review," *Desalination*, vol. 118, no. 1–3, pp. 81–89, Sep. 1998.

[35] R. W. Field, D. Wu, J. a. Howell, and B. B. Gupta, "Critical flux concept for microfiltration fouling," *Journal of Membrane Science*, vol. 100, no. 3, pp. 259–272, Apr. 1995.

[36] A. Fane and C. Fell, "A review of fouling and fouling control in ultrafiltration," *Desalination*, vol. 62, pp. 117–136, 1987.

[37] K. Zhang, H. Choi, D. D. Dionysiou, G. a Sorial, and D. B. Oerther, "Identifying pioneer bacterial species responsible for biofouling membrane bioreactors," *Environmental microbiology*, vol. 8, no. 3, pp. 433–40, Mar. 2006.

[38] M. Yamada, M. Nakashima, and M. Seki, "Pinched flow fractionation: continuous size separation of particles utilizing a laminar flow profile in a pinched microchannel," *Analytical chemistry*, vol. 76, no. 18, pp. 5465–71, Sep. 2004.

[39] E. Chmela, R. Tijssen, M. T. Blom, H. J. G. E. Gardeniers, and A. van den Berg, "A chip system for size separation of macromolecules and particles by hydrodynamic chromatography," *Analytical chemistry*, vol. 74, no. 14, pp. 3470–5, Jul. 2002.

[40] L. Huang, P. Silberzan, J. Tegenfeldt, E. Cox, J. Sturm, R. Austin, and H. Craighead, "Role of Molecular Size in Ratchet Fractionation," *Physical Review Letters*, vol. 89, no. 17, p. 178301, Oct. 2002.

[41] L. R. Huang, E. C. Cox, R. H. Austin, and J. C. Sturm, "Continuous particle separation through deterministic lateral displacement," *Science*, vol. 304, no. 5673, pp. 987–90, May 2004.

[42] K. Loutherback, K. S. Chou, J. Newman, J. Puchalla, R. H. Austin, and J. C. Sturm, "Improved performance of deterministic lateral displacement arrays with triangular posts," *Microfluidics and Nanofluidics*, vol. 9, no. 6, pp. 1143–1149, May 2010.

[43] H. Seo, H. Kim, and Y. Kim, "Hydrodynamics and magnetophoresis based hybrid blood cell sorter," in *14th International Conference on Miniaturized Systems for Chermistry and Life Sciences*, 2010, pp. 223–225.

[44] N. Pamme and A. Manz, "On-chip free-flow magnetophoresis: continuous flow separation of magnetic particles and agglomerates," *Analytical chemistry*, vol. 76, no. 24, pp. 7250–6, Dec. 2004.

[45] M. Senaha, R. Mitamura, M. Yamada, and M. Seki, "Two-dimensional cell sorting device employing pinched-flow fractionation and magnetophoresis," in *14th International Conference on Miniaturized Systems for Chermistry and Life Sciences*, 2010, pp. 1616–1618.

[46] R. Piazza, "Thermophoresis: moving particles with thermal gradients," *Soft Matter*, vol. 4, no. 9, p. 1740, 2008.

[47] D. Vigolo, R. Rusconi, H. a. Stone, and R. Piazza, "Thermophoresis: microfluidics characterization and separation," *Soft Matter*, vol. 6, no. 15, p. 3489, 2010.

[48] J. D. Adams and H. T. Soh, "Adjustable passband particle separation device," in *14th International Conference on Miniaturized Systems for Chermistry and Life Sciences*, 2010, pp. 205–207.

[49] J. Shi, D. Ahmed, X. Mao, S.-C. S. Lin, A. Lawit, and T. J. Huang, "Acoustic tweezers: patterning cells and microparticles using standing surface acoustic waves," *Lab on a chip*, vol. 9, no. 20, pp. 2890–5, Oct. 2009.

[50] C. Grenvall, P. Augustsson, J. Folkenberg, and T. Laurell, "Development of a point-of-care bovine live stock health control system using acoustophoresis," in *14th International Conference on Miniaturized Systems for Chermistry and Life Sciences*, 2010, pp. 127–129.

[51] J. Enger, M. Goksör, K. Ramser, P. Hagberg, and D. Hanstorp, "Optical tweezers applied to a microfluidic system," *Lab on a chip*, vol. 4, no. 3, pp. 196–200, Jun. 2004.

[52] E. Eriksson, J. Enger, B. Nordlander, N. Erjavec, K. Ramser, M. Goksör, S. Hohmann, T. Nyström, and D. Hanstorp, "A microfluidic system in combination with optical tweezers for analyzing rapid and reversible cytological alterations in single cells upon environmental changes," *Lab on a chip*, vol. 7, no. 1, pp. 71–6, Jan. 2007.

[53] D. E. Raymond, A. Manz, and H. M. Wldmer, "Continuous Sample Pretreatment Using a Free-Flow Electrophoresis Device Integrated onto a Silicon Chip," *Analytical chemistry*, vol. 66, no. 18, pp. 2858–2865, 1994.

[54] S. Köhler, H. Becker, V. Beushausen, E. Beckert, S. Howitz, and D. Belder, "Free-flow electrophoresis with electrode-less injection," in *14th International Conference on Miniaturized Systems for Chermistry and Life Sciences*, 2010, pp. 351–353.

[55] Y. Zhou and Q. Lin, "Microfluidic generation of temporally stable, flow-free profiles of chemical concentration gradients," in *14th International Conference on Miniaturized Systems for Chermistry and Life Sciences*, 2010, pp. 464–466.

[56] C. Zhang and A. Manz, "High-speed free-flow electrophoresis on chip," *Analytical chemistry*, vol. 75, no. 21, pp. 5759–66, Nov. 2003.

[57] B. R. Fonslow, V. H. Barocas, and M. T. Bowser, "Using channel depth to isolate and control flow in a micro free-flow electrophoresis device," *Analytical chemistry*, vol. 78, no. 15, pp. 5369–74, Aug. 2006.

[58] R. T. Turgeon and M. T. Bowser, "Micro free-flow electrophoresis: theory and applications.," *Analytical and bioanalytical chemistry*, vol. 394, no. 1, pp. 187–98, May 2009.

[59] Y. Zhang, R. Barber, and D. Emerson, "Particle Separation in Microfluidic Devices 3/4 SPLITT Fractionation and Microfluidics," *Current Analytical Chemistry*, vol. 1, no. 3, pp. 345–354, Nov. 2005.

[60] C. B. Fuh and J. C. Giddings, "Separation of submicron pharmaceutic emulsions with centrifugal split-flow thin (SPLITT) fractionation," *Journal of Microcolumn Separations*, vol. 9, no. 3, pp. 205–211, 1997.

[61] R. G. Keil, E. Tsamakis, C. B. Fuh, J. C. Giddings, and J. I. Hedges, "Mineralogical and textural controls on the organic composition of coastal marine sediments: Hydrodynamic separation using SPLITT-fractionation," *Geochimica et Cosmochimica Acta*, vol. 58, no. 2, pp. 879–893, Jan. 1994.

[62] S. Choi and J.-K. Park, "Microfluidic system for dielectrophoretic separation based on a trapezoidal electrode array," *Lab on a chip*, vol. 5, no. 10, pp. 1161–7, Oct. 2005.

[63] C. D. James, M. Okandan, S. S. Mani, P. C. Galambos, and R. Shul, "Monolithic surface micromachined fluidic devices for dielectrophoretic preconcentration and routing of particles," *Journal of Micromechanics and Microengineering*, vol. 16, no. 10, pp. 1909–1918, Oct. 2006.

[64] Z. Long, D. Liu, N. Ye, J. Qin, and B. Lin, "Integration of nanoporous membranes for sample filtration/preconcentration in microchip electrophoresis.," *Electrophoresis*, vol. 27, no. 24, pp. 4927–34, Dec. 2006.

[65] J. McDonald and G. Whitesides, "Poly (dimethylsiloxane) as a material for fabricating microfluidic devices," *Accounts of chemical research*, vol. 35, no. 7, pp. 491–499, 2002.

[66] A. Stroock and G. Whitesides, "Components for integrated poly (dimethylsiloxane) microfluidic systems," *Electrophoresis*, vol. 23, no. 20, pp. 3461–73, 2002.

[67] Z. Liu, Y. Zhang, J. Yu, and A. Mak, "A microfluidic chip with poly (ethylene glycol) hydrogel microarray on nanoporous alumina membrane for cell patterning and drug testing," *Sensors and Actuators B*, vol. 143, no. 2, pp. 776–783., 2010.

[68] J. Kim and B. Gale, "Quantitative and qualitative analysis of a microfluidic DNA extraction system using a nanoporous AlOx membrane," *Lab on a Chip*, vol. 8, no. 9, pp. 1516–1523, 2008.

[69] H. Osmanbeyoglu, T. Hur, and H. Kim, "Thin alumina nanoporous membranes for similar size biomolecule separation," *Journal of Membrane Science*, vol. 343, no. 1, pp. 1–6, 2009.

[70] J. de Jong, R. G. H. Lammertink, and M. Wessling, "Membranes and microfluidics: a review," *Lab on a chip*, vol. 6, no. 9, pp. 1125–39, Sep. 2006.

[71] S. Upadhyaya and P. Selvaganapathy, "Microfluidic devices for cell based high throughput screening," *Lab on a Chip*, vol. 10, no. 3, pp. 341–348, 2010.

[72] K. Aran, L. A. Sasso, N. Kamdar, and J. D. Zahn, "Irreversible, direct bonding of nanoporous polymer membranes to PDMS or glass microdevices," *Lab on a Chip*, vol. 10, no. 5, pp. 548–52, 2010.

[73] S. Noblitt, J. Kraly, and J. VanBuren, "Integrated membrane filters for minimizing hydrodynamic flow and filtering in microfluidic devices," *Analytical chemistry*, vol. 79, no. 16, pp. 6249–6254, 2007.

[74] J. M. K. Ng, I. Gitlin, A. D. Stroock, and G. M. Whitesides, "Components for integrated poly(dimethylsiloxane) microfluidic systems," *Electrophoresis*, vol. 23, no. 20, pp. 3461–73, Oct. 2002.

[75] H. Wu, X. Zhang, D. Xu, B. Li, and Z. Jiang, "Enhancing the interfacial stability and solvent-resistant property of PDMS/PES composite membrane by introducing a bifunctional aminosilane," *Journal of Membrane Science*, vol. 337, no. 1, pp. 61–69, Jul. 2009.

[76] Y. Gu and N. Miki, "A microfilter utilizing a polyethersulfone porous membrane with nanopores," *Journal of Micromechanics and Microengineering*, vol. 17, no. 11, pp. 2308–2315, Nov. 2007.

[77] K. Aran, L. A. Sasso, N. Kamdar, and J. D. Zahn, "Irreversible, direct bonding of nanoporous polymer membranes to PDMS or glass microdevices.," *Lab on a chip*, vol. 10, no. 5, pp. 548–52, Mar. 2010.

[78] J. N. Lee, C. Park, and G. M. Whitesides, "Solvent Compatibility of Poly(dimethylsiloxane)-Based Microfluidic Devices," *Analytical Chemistry*, vol. 75, no. 23, pp. 6544–6554, 2003.

[79] H. Wu, X. Zhang, D. Xu, B. Li, and Z. Jiang, "Enhancing the interfacial stability and solvent-resistant property of PDMS/PES composite membrane by introducing a bifunctional aminosilane," *Journal of Membrane Science*, vol. 337, no. 1, pp. 61–69, 2009.

[80] K. S. Lee and R. J. Ram, "Plastic-PDMS bonding for high pressure hydrolytically stable active microfluidics," *Lab on a chip*, vol. 9, no. 11, pp. 1618–24, Jun. 2009.

[81] M. A. Eddings, M. A. Johnson, and B. K. Gale, "Determining the optimal PDMS–PDMS bonding technique for microfluidic devices," *Journal of Micromechanics and Microengineering*, vol. 18, no. 6, p. 067001, Jun. 2008.

[82] L. Tang and N. Y. Lee, "A facile route for irreversible bonding of plastic-PDMS hybrid microdevices at room temperature," *Lab on a chip*, vol. 10, no. 10, pp. 1274–80, May 2010.

[83] S. Bhattacharya, A. Datta, J. M. Berg, and S. Gangopadhyay, "Studies on surface wettability of poly(dimethyl) siloxane (PDMS) and glass under oxygen-plasma treatment and correlation with bond strength," *Journal of Microelectromechanical Systems*, vol. 14, no. 3, pp. 590–597, Jun. 2005.

[84] I. Wong and C. Ho, "Surface molecular property modifications for poly(dimethylsiloxane) (PDMS) based microfluidic devices," *Microfluidics and nanofluidics*, vol. 7, no. 3, pp. 291–306, Sep. 2009.

[85] S. S. Madaeni and S. Hoseini, "Fabrication and characterization of PDMS coated PES membranes for separation of ethylene from nitrogen," *Journal of Polymer Research*, vol. 16, no. 5, pp. 591–599, Jan. 2009.

[86] A. Cordeiro, M. Nitschke, and A. Janke, "Fluorination of poly (dimethylsiloxane) surfaces by low pressure CF4 plasma-physicochemical and antifouling properties," *Polymer letters*, vol. 3, no. 2, pp. 70–83, 2009.

[87] S. Lee, S. H. Oh, and W. Lee, "The effect of direct fluorination of polydimethylsiloxane films on their surface properties.," *Journal of colloid and interface science*, vol. 332, no. 2, pp. 461–6, Apr. 2009.

[88] G. Corbin, R. Cohen, and R. Baddour, "Kinetics of polymer surface fluorination: Elemental and plasma-enhanced reactions," *Polymer*, vol. 23, no. 10, pp. 1546–1548, 1982.

[89] P. Rezai, "Plasma enhanced bonding of polydimethylsiloxane with parylene and its optimization," *Journal of Micromechanics and Microengineering*, vol. 21, no. 6, p. 065024, 2011.

[90] J. Hopkins and J. P. S. Badyal, "CF4 Plasma Treatment of Asymmetric Polysulfone Membranes," *Langmuir*, vol. 12, no. 15, pp. 3666–3670, 1996.

[91] M. Strobel, S. Corn, C. S. Lyons, and G. A. Korba, "Plasma fluorination of polyolefins," *Journal of Polymer Science Part A: Polymer Chemistry*, vol. 25, no. 5, pp. 1295–1307, May 1987.

[92] A. L. Thangawng, R. S. Ruoff, M. a Swartz, and M. R. Glucksberg, "An ultra-thin PDMS membrane as a bio/micro-nano interface: fabrication and characterization.," *Biomedical microdevices*, vol. 9, no. 4, pp. 587–95, Aug. 2007.

Appendix A - Photolithography Mold Fabrication

1) Obtain 3" silicon wafer and clean using acetone, isopropyl alcohol, ethanol, methanol and DI water

2) Dry using nitrogen gas to blow off excess liquid and dry on hot plate at 95°C

3) Place 3" wafer chuck on spinner, place wafer on center of chuck, turn on vacuum to hold wafer

4) Pour 2-3 ml of SU-8 photoresist on silicon wafer.

5) Spin at 500 rpm for 5 - 10 sec with acceleration of 100 rpm/sec

6) Increase to 4000 rpm at an acceleration of 300 rpm/s and continue spinning for 1 min at the final speed. Remove wafer.

7) Place wafer on hotplate and soft-bake the wafer at 65°C for 1 min 17 sec

9) Transfer to 95°C hot plate and hard bake for 95°C for 7 min 17 sec

10) Check for wrinkles. If wrinkles are present, continue hard bake until wrinkles are gone.

11) Preheat filament in mask aligner and mount the mask on the mask aligner. Masks are designed through CAD design programs and printed by ARTCAD.

12) Put the wafer on the wafer holder of mask aligner and align with the mask using adjustment knobs. Once aligned, bring mask and wafer into contact.

14) Expose the wafer to UV light for a total exposure energy of 177.86 mJ/cm^2

15) Soft-bake the wafer at 65°C for 1 min 25 sec

16) Hard-bake the wafer at 95°C for 6 min 25 sec

17) Place wafer in SU-8 developer for 10 min while gently shaking the developer

18) Rinse the wafer with IPA for 1 min and wash with DI water. Dry using nitrogen gas.

19) If there is a white residue on the wafer, repeat step 17 and 18.

20) Check dimensions and height of features using Alpha Step Profilometer

21) Continue hard baking at 95°C for overnight to ensure optimal hardness.